MICROCOPY RESOLUTION TEST CHART
NATIONAL BUREAU OF STANDARDS 1963 A

MULTILAYER CAPACITOR DIELECTRICS PRODUCED FROM

METALLO-ORGANIC PRECURSORS

R.W. Vest and G.M. Vest

Purdue University

W. Lafayette, IN

30 June 1985
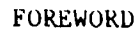
Annual Report

For the Period 3/1/85 - 3/31/86

Contract No. N00014-83-K-0321

Prepared for: Office of Naval Research

86 7 28 169

FOREWORD

The research described in this report was conducted under Contract No. N00014-83-K-0321 with the Office of Naval Research under the technical cognizance of Dr. R.C. Pohanka. Research was conducted in the Turner Laboratory for Electroceramics, School of Materials Engineering and School of Electrical Engineering, Purdue University, West Lafayette, Indiana under the direction of R.W. Vest and G.M. Vest. Contributing to the project were Dr. S. Singaram and Messrs. A.K. Bhansali, D.A. Binford, R.L. Reed, A.S. Shaikh, and J.J. Xu.

TABLE OF CONTENTS

1. INTRODUCTION

The metallo-organic decomposition (MOD) process for preparing films or powders has a number of advantages over conventional processes. The metallo-organic compounds used in the present study had oxygen as the hetero atom to bond a metal atom to an organic ligand. These compounds were each dissolved in an appropriate solvent and the solutions mixed to achieve the desired stoichiometry. After adjusting the rheology, the formulation was deposited on an appropriate substrate to make a film or contained in a platinum dish to make a powder, and pyrolyzed too yield the inorganic product. Since the mixing of the starting materials is on the molecular level, the inorganic species exist as atoms or molecules in intimate contact immediately after decomposition. This leads to much more rapid formation of compounds and sintering of films, which translates to lower temperature processing of equilibrium phases and more dense films.

This report is divided into three parts. The first details studies of the formation of $PbTiO_3$ films by the MOD process, and demonstrates that defect free films 0.5 to 2.0 μm thick can be prepared over 2 cm X 2 cm areas. The second part of the report describes a study of grain size effects on the dielectric properties of $BaTiO_3$. The use of the MOD process gave 45 nm powders which were pressed and sintered to give ceramic bodies with controlled grain size. The third part of the report discusses preliminary studies of the formation of lead magnesium niobate by the MOD process.

2. PREPARATION AND PROPERTIES OF PbTiO$_3$ FILMS

2.1 General

Lead titanate (PbTiO$_3$) is one of the most polar ferroelectrics with a Curie point of 490°C [1]. However, very little is known about the intrinsic properties due to the difficulty in growing single crystals of appreciable size. PbTO$_3$ single crystals grown by the aid of KF flux [2] showed a tetragonal lattice with c = 04150 nm and a = 03904 nm. The spontaneous polarization is high at room temperature; some authors suggest the value of P$_s$ to be greater than 50 μC/cm^2 [2,3]. The relative permittivity in an a.c. field of 10 kHz is about 10000 in the neighborhood of the Curie temperature [2]. Modified PbTiO$_3$ ceramics have been investigated extensively for high-temperature and high-frequency applications [4-6]. The excellent piezoelectric properties of PbTiO$_3$ ceramics, due to their very small aging rate of dielectric constant [7] and large anisotropy in piezoelectric constant between longitudinal and transverse modes, have been utilized in practical electronic device applications [8-10].

The preparation of PbTiO$_3$ thin films provides a unique opportunity to control either the composition or the structure in such a manner as to give useful non-bulk properties to the resultant film. The principal useful property is the dimension of the structure perpendicular to the substrate. Thin films of amorphous PbTiO$_3$ prepared by RF sputtering on cooled substrates [11] contained Pb-metal cyrstallites that showed a tendency to increase toward the surface and caused a high electrical

conductivity. Another problem with the sputtering is that is was found to be difficult to control the composition of the film [12]. The surfaces of films produced by chemical vapor desposition [13] were much smoother than those prepared by RF sputtering.

The metallo-organic decomposition (MOD) process used to grow $PbTiO_3$ thin films discussed in this section has a number of advantages over conventional processes. Different types of MOD films have been discussed in various papers and technical reports by the Vests [14-18]. The metallo-organic compounds used in the present study had oxygen as the hetero atom bridge between a metal atom and an organic ligand. These compounds were each dissolved in an appropriate solvent and the solutions mixed to achieve the desired stoichiometry. The homogeneous solutions were spun onto the substrates to form uniform wet films, which were then heated to produce the desired inorganic phase. Since the mixing of the starting materials is on the molecular level in the solution, the inorganic species exist as atoms or molecules in intimate contact immediately after decomposition, which leads to rapid formation of compounds in films and lower temperature processing of equilibrium phases. Thus, the MOD technique has great potential of overcoming the difficulties encountered with other techniques for film formation.

2.2 Experimental

2.2.1 Materials Selection and Synthesis

2.2.1.1 Selection of Compounds

Lead neodecanoate $[Pb(C_9H_{19} \quad {}_2]$ and titanium di-methoxy-di-neodecanoate $[(CH_3O)_2Ti(C_9H_{19}COO)_2]$ were the precursors used for $PbTiO_3$. Platinum amine 2-ethylhexanoate $[Pt(C_3H_{10}N_2)_2(C_7H_{15}COO)_4]$ was chosen to produce a thin Pt film on Si-wafer substrates. To increase the adhesion between the Pt film and the substrate, a small amount of bismuth was added to the platinum amine 2-ethylhexanoate solution in the form of bismuth 2-ethylhexanoate $[Bi(C_7H_{15}COO)_2]$. The above choices of metallo-organic compounds for the MOD process were based on the following requirements: high metal content; high solubility in common oganic solvents; thermally decompose without melting or evaporating; stable under ambient condition (e.g. do not gel); and compatible with other compounds in the formulation. The specific compounds selected were a compromise among these various requirements. All the metallo-organic compounds used in this study were synthesized in house for better control over experimental variables.

2.2.1.2 Titanium Di-Methoxy-Di-Neodecanoate

Eighty six grams (0.5 moles) of titanium methoxide was transferred to a 1000 ml flask under an inert atmosphere. Two hundred ml (1 mole) of 95% pure neodecanoate acid and about 20 ml of pure methanol were added to the flask without disturbing the inert atmosphere. The reaction mixture was refluxed under the inert atmosphere for about three hours at $65^{\circ}C$. A pale yellow viscous liquid was obtained. Methanol was

removed by vacuum distillation, and the liquid was dissolved in xylene.
Reaction:

$$(CH_3O)_4Ti + 2C_9H_{19}COOH \rightarrow (CH_3O)_2Ti(C_9H_{19}COO)_2 + 2CH_3OH$$
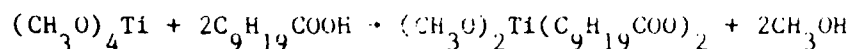
2.2.1.3 Lead Neodecanoate

Two hundred and fourty grams (0.73 moles) of $Pb(NO_3)_2$ were dis-
solved in 700 ml of water. In a 2000 ml beaker, 280 ml (1.4 moles) of
neodecanoic acid (95% purity) was neutralized with 87 ml of NH_4OH (NH_3
assay: 30%). After stirring the solution for 20-25 minutes, the
$Pb(NO_3)_2$ solution was added with constant stirring. A pale yellow,
gummy lead neodecanoate soap settled to the bottom of the flask. It was
separated from the aqueous solution and dissolved in xylene. Reactions:

$$NH_4OH + C_9H_{19}COOH \rightarrow C_9H_{19}COONH_4 + H_2O$$

$$2C_9H_{19}COONH_4 + Pb(NO_3)_2 \rightarrow 2NH_4NO_3 + Pb(C_9H_{19}COO)_2$$
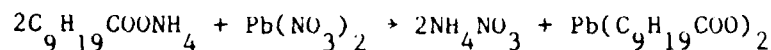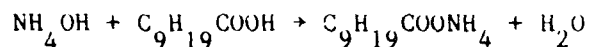
2.2.1.4 Platinum Amine 2-Ethylhexanoate

In a round bottomed flask, 1.54 g (0.0029 moles) of $H_2PtCl_6 \cdot 6H_2O$
was dissolved in absolute methanol (8 ml) and cooled in an ice-bath (0-
$5°C$). To this, 1.28 grams (0.0074 moles) of 1,2-diammino propane was
added dropwise and stirred for 0.5 hours. The precipitate was washed
with methanol and then dissolved in deionized water. An ammonium salt

of 2-ethylhexanoate acid was prepared by mixing 2.7 grams (0.019 moles) of 2-ethylhexanoic acid and 1.26 ml of 58% ammonium hydroxide in a 100 ml flask. With continuous stirring, the aqueous platinum amine solution was added dropwise at room temperature, and this mixture was stirred for 2 hours. A yellow oily portion at the bottom was separated and extracted in xylene (~10 ml). Reactions:

$$H_2PtCl_6 \cdot 6H_2O + 4C_3H_{10}N_2 \rightarrow Pt(C_3H_{10}N_2)_2Cl_4 + 2C_3H_{10}N_2 \cdot HCl + 6H_2O$$

$$C_7H_{15}COOH + NH_4OH \rightarrow C_7H_{15}COONH_4 + H_2O$$

$$Pt(C_3H_{10}N_2)_2Cl_4 + 4C_7H_{15}COONH_4 \rightarrow 4NH_4Cl + Pt(C_3H_{10}N_2)_2(C_7H_{15}COO)_4$$
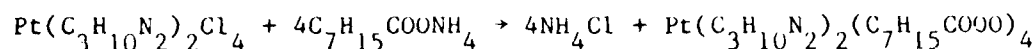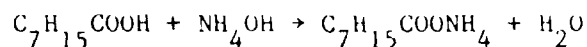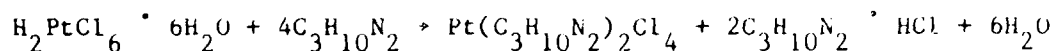
2.2.1.5 Bismuth 2-Ethylhexanoate

A mixture of 6.4 ml (0.004 moles) of 2 ethylhexanoic aicd and 4 ml (0.06 moles) of 58% ammonium hydroxide in 25 ml of water was stirred. Five grams (0.01 moles) of $Bi(NO_3)_3 \cdot 5 H_2O$ in 10% NHO_3 was added slowly to the solution. The reacted oily portion was separated and dissolved in xylene. Reactions:

$$NH_4OH + C_7H_{15}COOH \rightarrow C_7H_{15}COONH_4 + H_2O$$

$$Bi(NO_3)_3 5H_2O + 3C_7H_{15}COONH_4 \rightarrow Bi(C_7H_{15}COO)_3 + 3NH_4NO_3 + H_2O$$
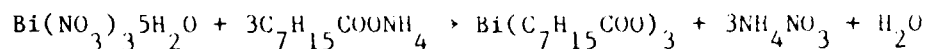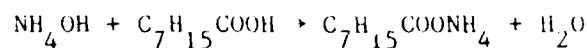
2.2.2 Substrates

Two kinds of substrates were used in this study. Pure Pt foil was used mainly to study the crystal structure and phase transformations for the $PbTiO_3$ films for various experimental variables since it will limit the chemical impurity effects. However, the difference of thermal expansion between Pt and polycrystalline $PbTiO_3$ ($\alpha = 8.9 \times 10^{-6}/^{\circ}C$ and $-3.3 \times 10^{-6}/^{\circ}C$ for Pt and $PbTiO_3$, respectively [19]) made it difficult to form even a small area of crack-free film for studies of the electrical properties. Multilayer-Pt-coated Si wafers (p type, 111 orientation) were also used as substrates because the improved thermal expansion match between $PbTiO_3$ and Si ($\alpha = 2.6 \times 10^{-6}$ at room temperature [19]) made it possible to form nearly crack-free $PbTiO_3$ films 2 cm X 2 cm.

2.2.3 Control of Film Thickness

The thickness of single layer $PbTiO_3$ films on the substrates was found to have considerable effect on features such as crystal structure, grain size, relative amount of residual amorphous phase and the suface roughness of the fired films. In addition, the mismatch of thermal expansion between film and substrate also requires careful control of film thickness in order to get crack free films. For this study, the conventional spinning technique was used to form a uniform wet film on the substrate. The spinning was carried out in a Class 100 hood in order to minimize dust particle streaks in the films. The film

thickness was established by controlling the spinning speed and time, and the viscosity of the solution of metallo-organic compounds. Figure 2.1 illustrates the effect of spinnng speed, and Fig. 2.2 shows the effect of the concentration of the metallo-organic compounds in solution on both film thickness and viscosity of the solution.

2.2.4 Firing

All samples were fired in a fused quartz muffle furnace with an air atmosphere. A programmable control unit was used to establish the time-temperature profile. Some of the samples were fired in a D.C. electrical field from 2.5 kV/cm to 8.5 kV/cm, which was established by two parallel stainless steel plates. Generally, the heating rate and the maximum firing temperature were found to effect the realtive amount of amorphous $PbTiO_3$ and the formation of undesired pyrochlore phase. The thermal analysis of $Pb(C_9H_{19}OO)_2$ and $Ti(CH_3O)_2(C_9H_{19}COO)_2$ at a heating rate of $10^{\circ}C$/minute showed that the reactions

$$Pb(C_9H_{19}COO)_2 \rightarrow PbO$$

and

$$Ti(CH_3O)_2(C_9H_{19}COO)_2 \rightarrow TiO_2$$
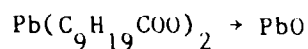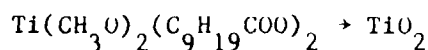
were both complete at almost the same point: $370^{\circ}C \pm 2^{\circ}C$. Therefore, the majority of the studies of the effects of different time-temperature profiles were carried out below $370^{\circ}C$.

Viscosity (mPa.s)

Spinning speed: 3000 RPM
Spinning time: 30 sec.

O thickness
● viscosity

20.0   15.0   10.0   5.0   0.0

14.5   13.0   11.5   10.0

Concentration (wt%)

0.40   0.30   0.20   0.10   0.0

Thickness (μm)

Figure 2.2   The dependence of single layer thickness
and viscosity of the solution of metallo-
organic compounds on the concentration
of the solution.

Spinning time: 30 sec.
Viscosity: 3.080 mPa.s

3000   2000   1000

Spinning Speed (RPM)

0.25   0.20   0.15   0.10

Thickness (μm)

Figure 2.1   The dependence of single layer
thickness on spinning speed.

2.2.5 Electrodes

The electrode between the $PbTiO_3$ film and the Si wafer had to be a continuous film with good electrially conductive, low surface roughness and good adhesion to the substrate. To achieve these requirements, a multi-layer MOD technique was used to form four-layer Pt films on the Si wafers. It was determined that the desired surface finish could only be achieved if each layer produced a fired thickness of ~12.5 nm. Platinum amine 2-ethylhexanoate $(Pt(C_3H_{10}N_2)_2 \ (C_7H_{15}COO)_4)$ was dissolved in tetrahydrofuran $(CH_2 \ (CH_2)_2 \ CH_2O)$ to form a solution containing 0.8 wt% Pt. The solution used to form the first layer on the Si wafer also contained Bi 2-ethylhexanoate in an amount such that the composition of the fired films was 5 wt% Bi_2O_3 and 95 wt% Pt. The geometry of a four-layer Pt film with total thickness 50 nm on a Si wafer is illustrated in Fig. 2.3(a). The sheet resistance measured by the Van Der Pauw method was 12 Ω/sq. To study the electrical properties of the $PbTiO_3$ films, planar capacitors were formed by vacuum evaporation of gold through a mask having holes of 1 mm in diameter. The planar capacitor structure is shown in Fig. 2.3(b).

2.2.6 Crystal Structure and Microstructure

X-ray diffraction analyses using CuK_α radiation were used to study phase formation and transformations, grain size, lattice parameters, and the preferred orientation of crystal growth. The microstructure of the films was studied using SEM and TEM.

Pt

5 wt% Bi₂O₃ + Pt

600 Å

Si Wafer Substrate

(a)

Gold dots

PbTiO₃ film

Pt film

Si Wafer Substrate

(b)
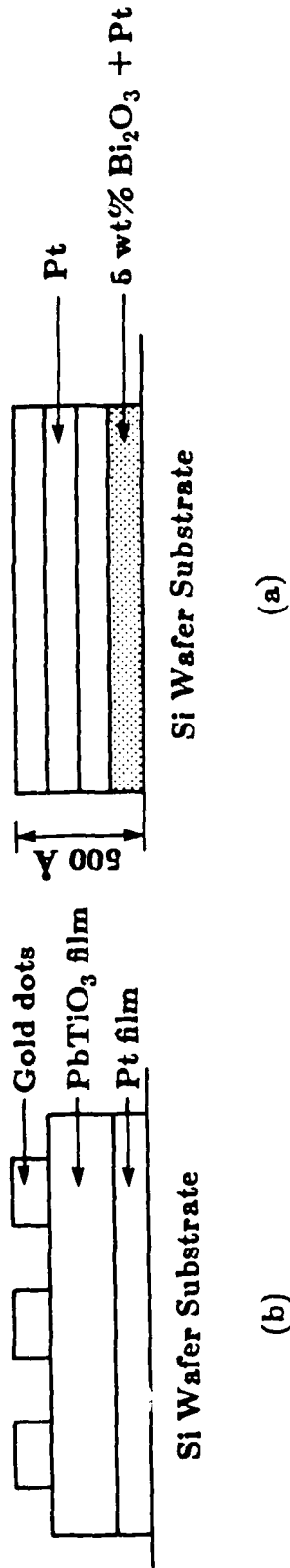
Figure 2.3 (a) The structure of the multilayer Pt film. (b) The planar capacitor structure.

2.2.7 Electrical Property Measurements

The temperature dependences of dielectric constant, dissipation factor and D.C. resistivity for $PbTiO_3$ films were studied from room temperature to $500^\circ C$. The dielectric constant and dissipation factor were measured using an LCR meter (HP 4262) at a frequency of 1 kHz and field strength 5 kV/cm to 12 kV/cm depending on the film thickness. The D.C. resistivity was measured using a Keithley 173 A multimeter, which has a useful range to 300 MΩ. At temperatures above $500^\circ C$, the high conductivity of the samples made it difficult to measure dielectric constant and dissipation factor. The ferroelectric hysteresis loop was displayed on an oscilloscope using a modified Saywer and Tower circuit [20].

2.3 Results and Discussion

2.3.1 Morphology of Films

The surface roughness of films formed using the same time-temperature profile was found to be directly related to the single layer thickness. Figure 2.4 shows the surface profiles for two single layer samples with thickness of 123 and 365 nm, respectively. The surface roughness is ~4 nm for the thinner sample and ~8 nm for the thicker sample (the Si wafer substrate had ~1 nm roughness). These surface finishes are much improved compared to films prepared by RF sputtering [11,12]. Figure 2.5 shows SEM pictures for the same samples. The film 123 nm thick (Fig. 2.5(a)) is a crack-free uniform film. In constrast,

(a)

(b)

μm
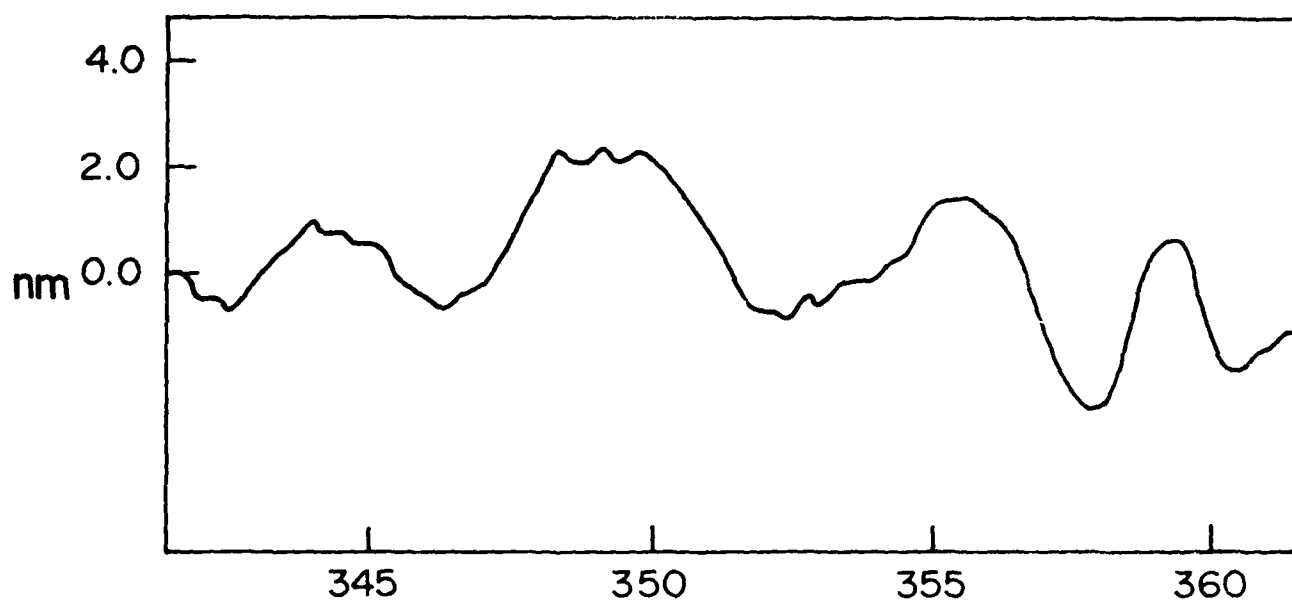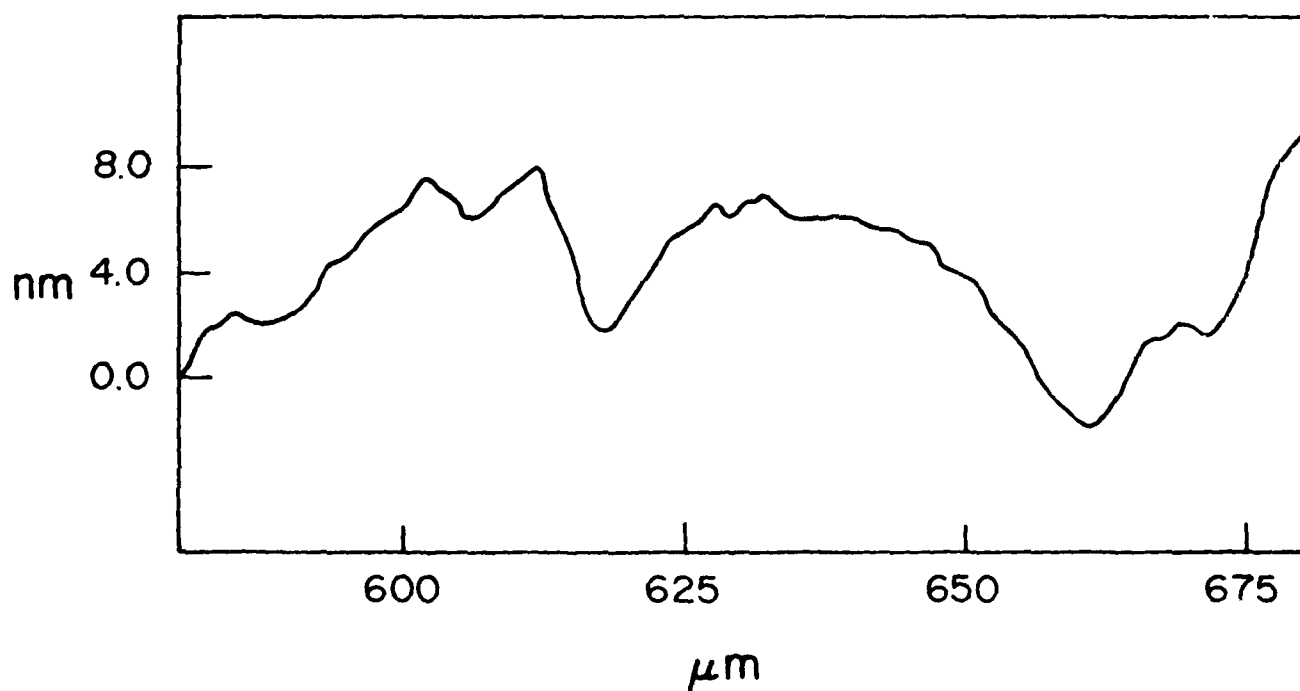
Figure 2.4   The surface profile for single layer PbTiO$_3$ film with identical thermal processing with thickness (a) 123 nm and (b) 365 nm.

there are severe cracks on the surface of the film 365 nm thick (Fig. 2.5(b)). The cracking is the result of the large volume change in going from the wet film to the fired film. This volume change may be as much as a factor of 30 depending on the concentration of the metallo-organic compounds in solution. Thicker films require a much slower heating rate through the critical temperature ranges. For a given time-temperature profile, the film must be below some critical thickness in order to sustain the volume change without cracking. Figure 2.6 shows the cross-section of a typical structure of five layer $PbTiO_3$ deposited on a four layer Pt coated Si wafer. The very dense $PbTiO_3$ film produced by the MOD technique is apparent.

2.3.2 Metastable Phase in the $PbO-TiO_2$ System

A metastable phase was observed in $PbTiO_3$ films (~1 μm thick) deposited on pure Pt foil. Figure 2.7 shows the x-ray diffraction patterns for the films at various firing temperatures. For films fired at $494^\circ C$ or lower, the x-ray diffraction patterns showed that the tetragonal phase was the only crystal structure formed (of course there existed a certain amount of amorphous $PbTiO_3$). As the firing temperature was raised to $514^\circ C$, a new crystal structure with $2\theta = 30.40^\circ$, 35.20° and 50.64° was formed. The realtive intensities of those peaks compared to the tetragonal peaks reached a maximum when the film was fired at $540^\circ -550^\circ C$. Further increasing the firing temperature decreased the relative intensity of the peaks of this metastable phase. Samples fired at $630^\circ C$ or higher showed no metastable phase. The lattice parameter and the (h,
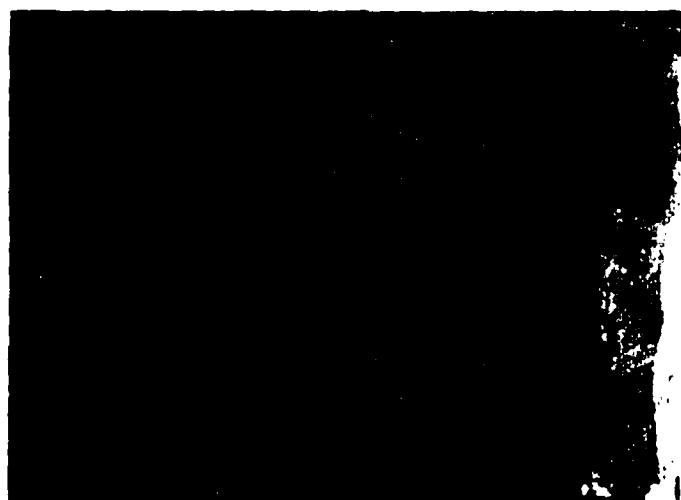
Figure 2.6   Micrograph (TEM) of the cross-section of substrate, Pt and PbTiO$_3$ film. (90,000 X).
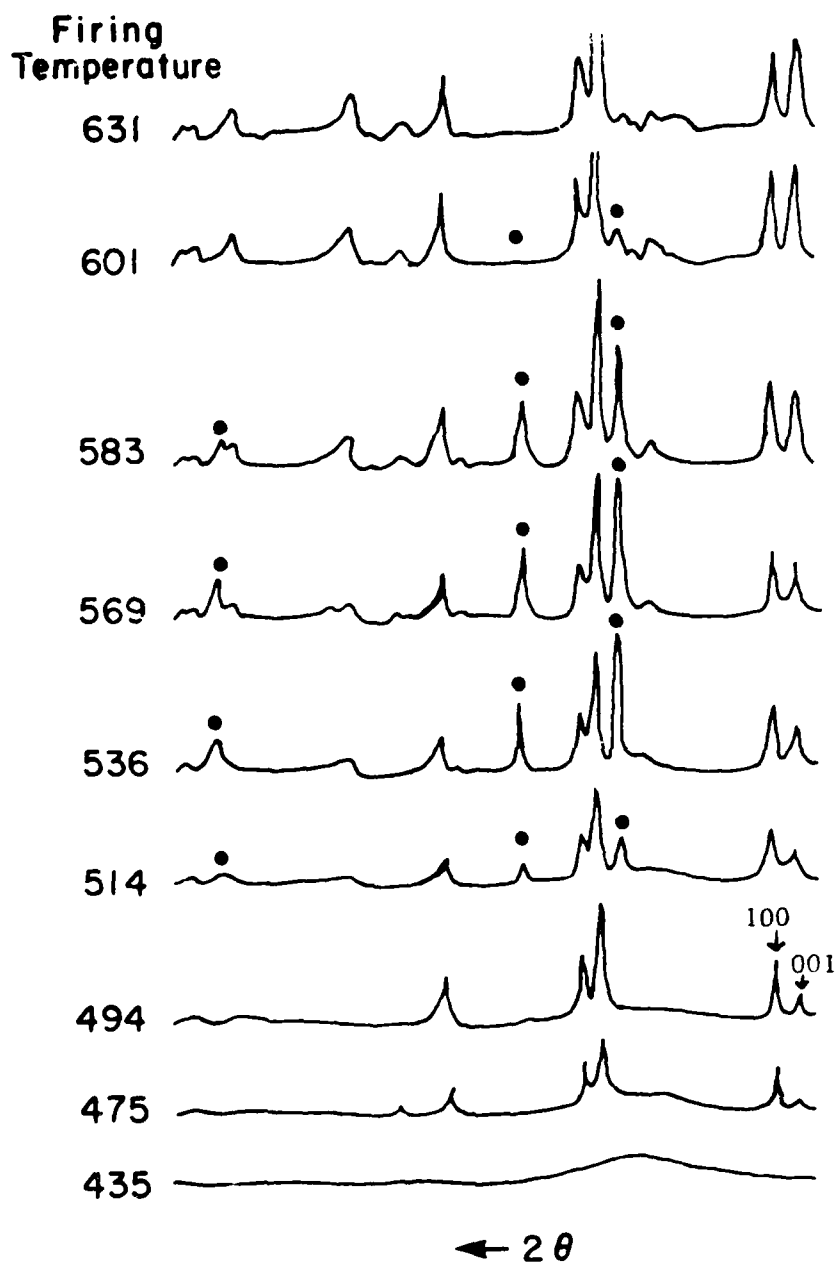
Figure 2.7 X-ray diffraction patterns (with CuK$_\alpha$) for films (1 µ) fired on Pt foil at various temperatures. The indicated peaks are not characteristic of tetragonal PbTiO$_3$.

k, l) values for $2\theta = 20.40°$, $35.20°$ and $50.64°$ were calculated assuming

that the metastable phase had the crystal symmetry Fd3m as did the pyro-

chlore structure observed in the $PbO-TiO_2-SiO_2$ system [21]. Each unit

cell of such a structure contains eight formulae of $Pb_2Ti_2O_6$. The posi-

tion of Pb ions are fixed in the lattice of d subgroup and Ti ions in c

sub-group [22]. For x-ray diffraction, the smallest value of $h^2+k^2+l^2$

is when $h=k=l=2$. Thus, it is confirmed that the smallest value of 2θ

$(30.40°)$ is the reflection from the $(2,2,2)$ plane. Thus, the lattice

parameter a can be calculated as:

$$d_{2,2,2} = \frac{\lambda}{2\,\sin\theta} = 0.24902 \text{ nm}$$

$$a = d_{2,2,2}\sqrt{h^2+k^2+l^2} = 1.019 \text{ nm}$$

The h,k,l values for $2\theta = 35.20°$ and $50.64°$C were calculated by

$$h^2+k^2+l^2 = (\frac{a}{d_{h,k,l}})^2$$

and it was found that $h^2+k^2+l^2 = 16$ and 32 for $2\theta = 35.20°$ and $50.64°$,

respectively. Considering the c,d subgroup's limitations, the peaks at

$2\theta = 35.20°$ and $50.64°$ must be reflections from $(4,0,0)$ and $(4,2,2)$

planes, respectively.

By the proper choice of firing conditions, the amount of amorphous

phase formed in the films could be minimized. X-ray diffraction pat-

terns for samples fired so as to minimize the formation of amorphous

phase indicated no metastable phase peaks, as shown in Fig. 2.8. The

pyrochlore phase was also never observed if the films were fully

(a)

(b)

2θ
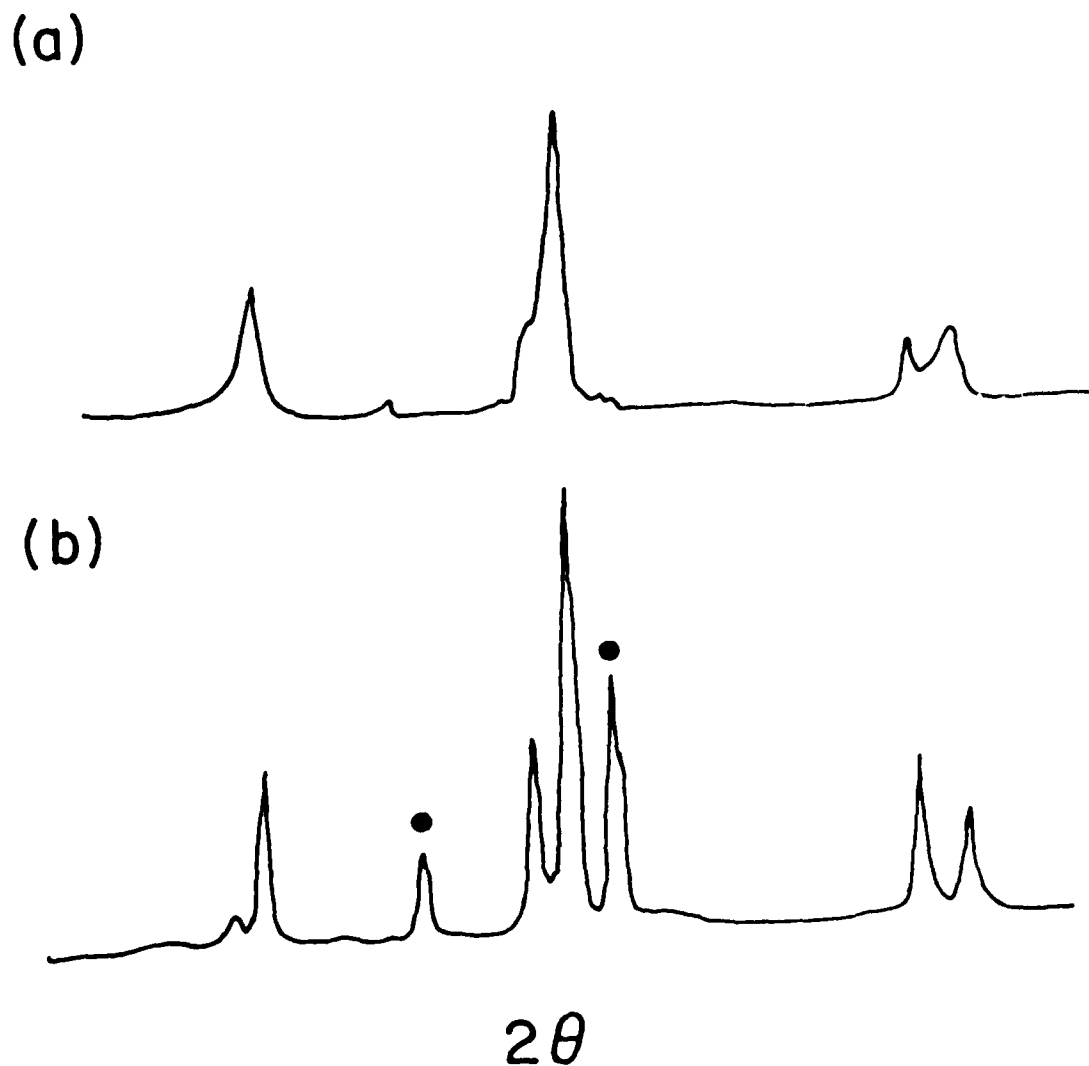
Figure 2.8   X-ray diffraction patterns (with CuK$_\alpha$) for films fired at
560°C with the thermal processing (a) to minimize the
formation of amorphous phase, (b) to maximize the formation of
amorphous phase. The indicated peaks are not characteristic
of tetragonal PbTiO$_3$.

crystallized from the amorphous phase below 500°C. The metastable phrochlore phase of $Pb_2Ti_2O_6$ can be formed only from amorphous $PbTiO_3$, and the tetragonal phase can not be transformed into the cubic phase at any temperature. The phase transformation diagram for the $PbTiO_3$ system is shown in Fig. 2.9.

2.3.3 Structure of Tetragonl $PbTiO_3$ Films

The axial ratio (c/a) for bulk tetragonal $PbTiO_3$ varies from 1.065 at 25°C to 1.02 at the Curie temperature (490°C) [23]. It was found that the c/a values for films fired at the same temperature changed with single layer thickness. Figure 2.10 shows that this ratio increases as the layer thickness increases, but in all cases was smaller than that of bulk tetragonal $PbTiO_3$

For the same thickness films fired at the same temperature, it was found the c/a values for those films fired in a D.C. electric field at temperatures below T_c were smaller compared to those fired without a field, and the effect increased with increasing field strength. Figure 2.11 shows the experimental results. The field strength dependence of c/a value can be explained if it is assumed that the dipole moment of the tetragonal $PbTiO_3$ unit cell is proportional to its axial ratio c/a. In an electrical field E, the energy density stored in a dielectric can be expressed as 1/2 PE, where P is the polarization or the dipole moment per unit volume. The smaller c/a will reduce the energy stored in the system thus giving a more stable state at thermal equilibrium. The phenomenon observed presents an opportunity to control the value of c/a,
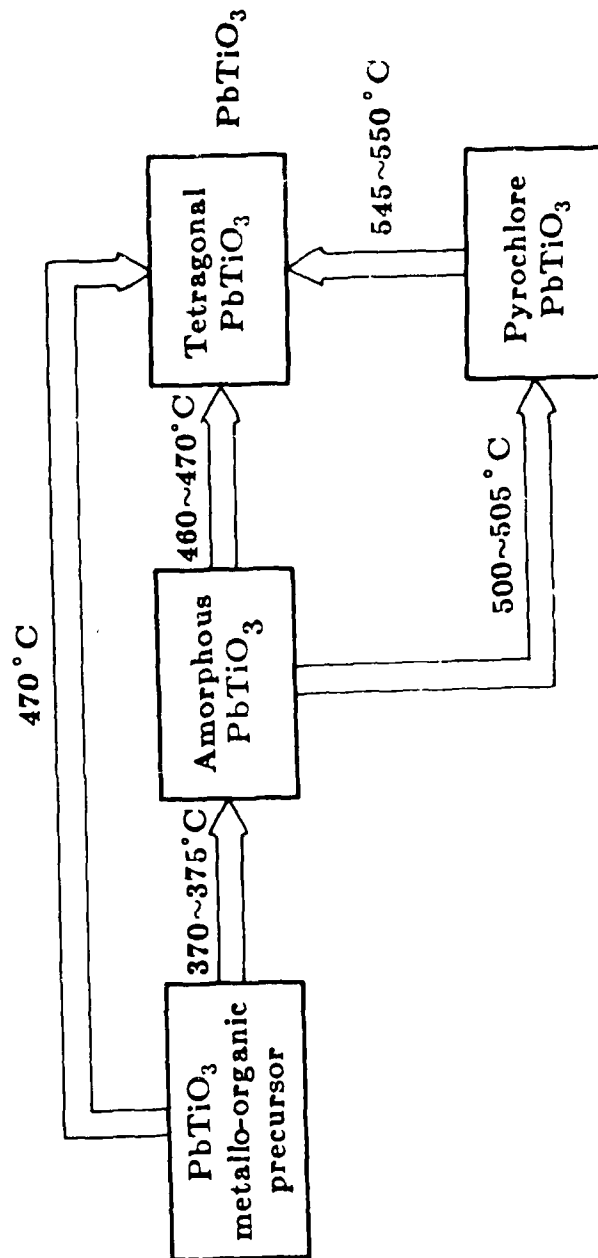
Figure 2.9 Phase transformation diagram for the PbTiO₃ system prepared by the MOD process.

470°C

370~375°C

Tetragonal PbTiO₃

460~470°C

Amorphous PbTiO₃

545~550°C

500~505°C

Pyrochlore PbTiO₃

PbTiO₃ metallo-organic precursor

c/a

Firing Temperature 552 °C
Firing Time: 8 hrs.

Single Layer Thickness (μm)
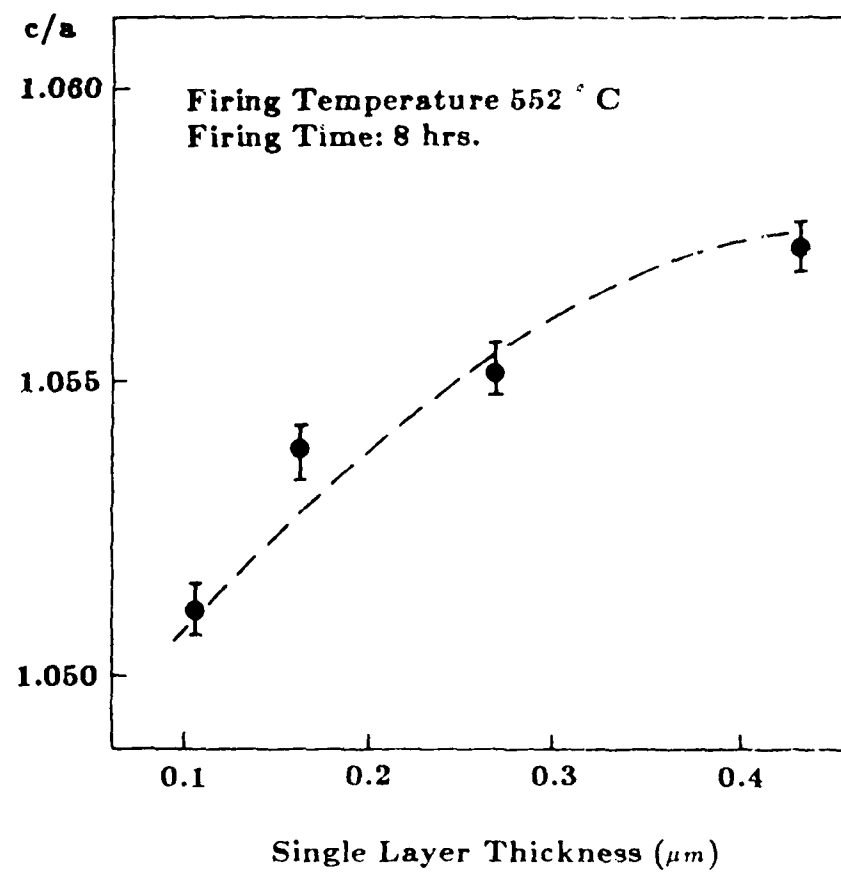
Figure 2.10 The dependence of c/a on the single layer thickness.
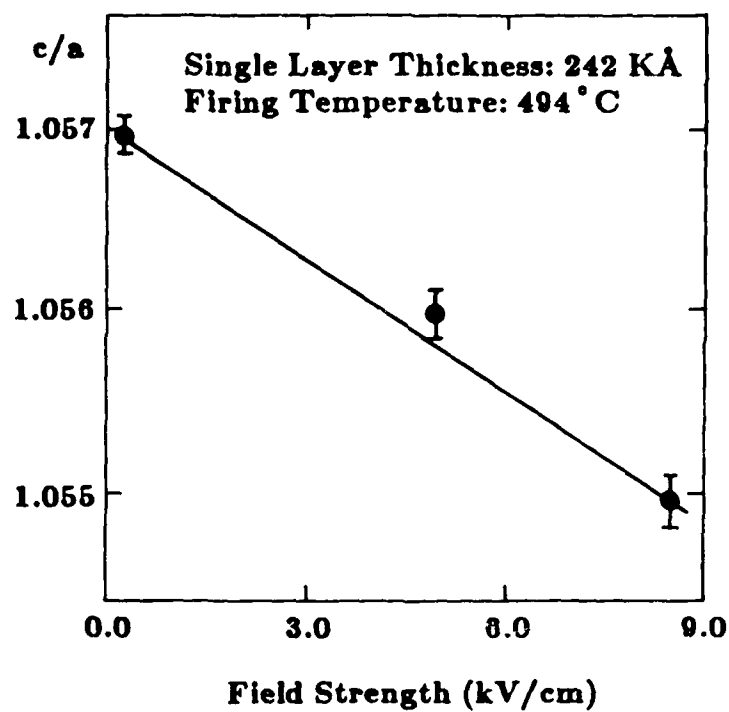
Figure 2.11   The dependence of c/a on C.D. electrical field strength
during firing for the film with 2.42 kA in single layer
thickness.
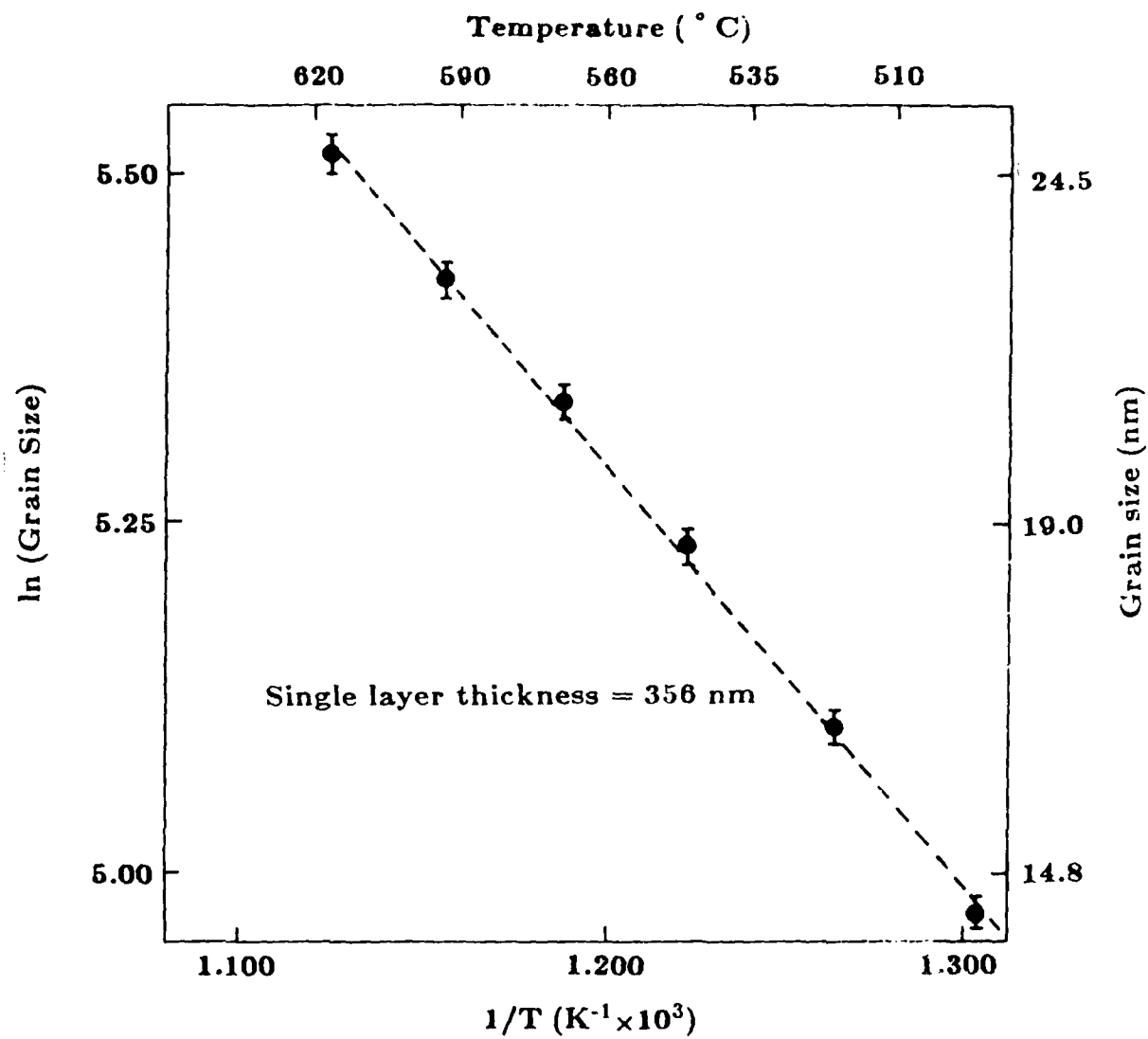
Figure 2.12   The grain size dependence of PbTiO$_3$ films on firing temperature.
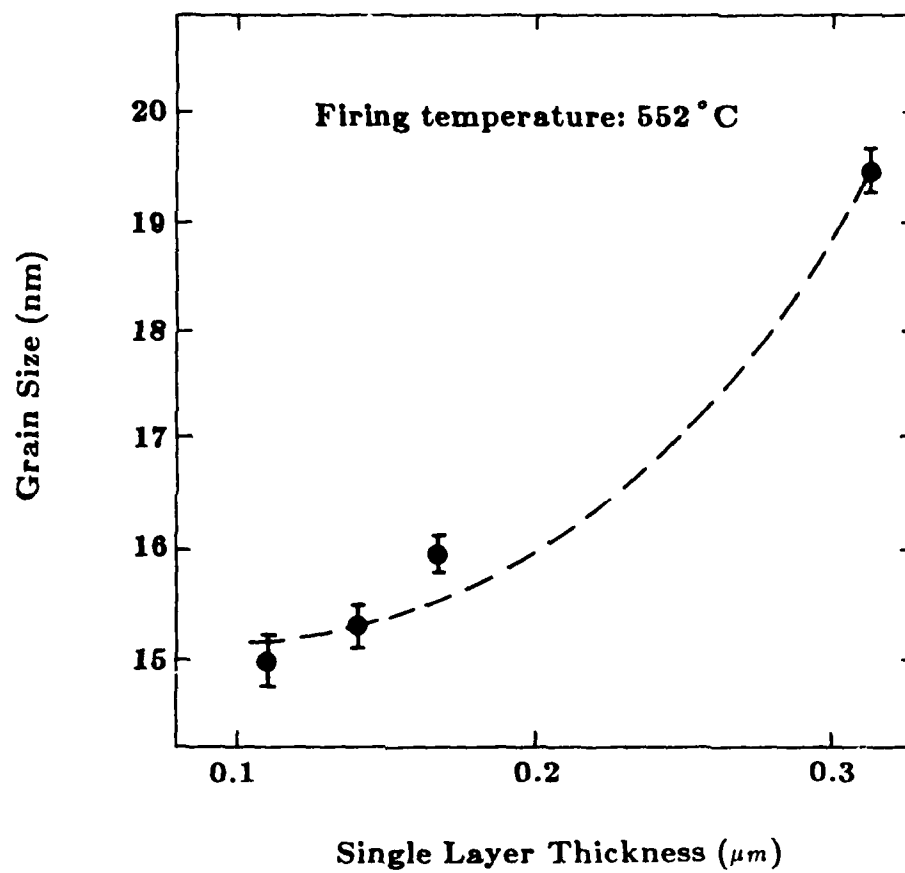
Figure 2.13 The grain size changes with single layer thickness for the films fired at $552^{\circ}C$.

In general, the polycrystalline PbTiO$_3$ films formed by the MOD technique showed a random orientation of grains. However, as the firing temperature was increased, the films indicated a preferred growth direction with the c axis (001) perpendicular to the substrate surface. As shown in Fig. 2.7, the peak intensity ratio of (001) to (100) is about 1:2 for the films fired at 500°C, which means that the c axes of the grains in the film were randomly distributed. This ratio increased as the firing temperature increased and reached 1.2:1 for the films fired at 630°C. The increase in this ratio means more grains direct their c axis perpendicular to the substrate. Further efforts to grow films in which all of the grains direct their c axis perpendicular to substrate are currently in process.

2.3.5 Electrial Properties

2.3.5.1 Dielectric Constant and Dissipation Factor

The room temperature dielectric constant of the planar capacitor structures (Fig. 2.3(b)) was found to be a strong function of relative humidity, as shown in Fig. 2.14. The origin of this effect is unknown, but its magnitude is impressive. Subsequent data were collected above 50°C were the effect of relative humidity is negligible. Figure 2.15 shows the temperature dependence of the dielectric constant and dissipation factor in the range 50° to 500°C for a tetragonal PbTiO$_3$ film 1.83 µm thick (six layers each 305 nm thick). A dielectric constant was 100 ~ 110 at temperatures below 300°C, and reached its maximum value of 3 X 10^4 at the Curie point. The measured Curie temperature was 493 to
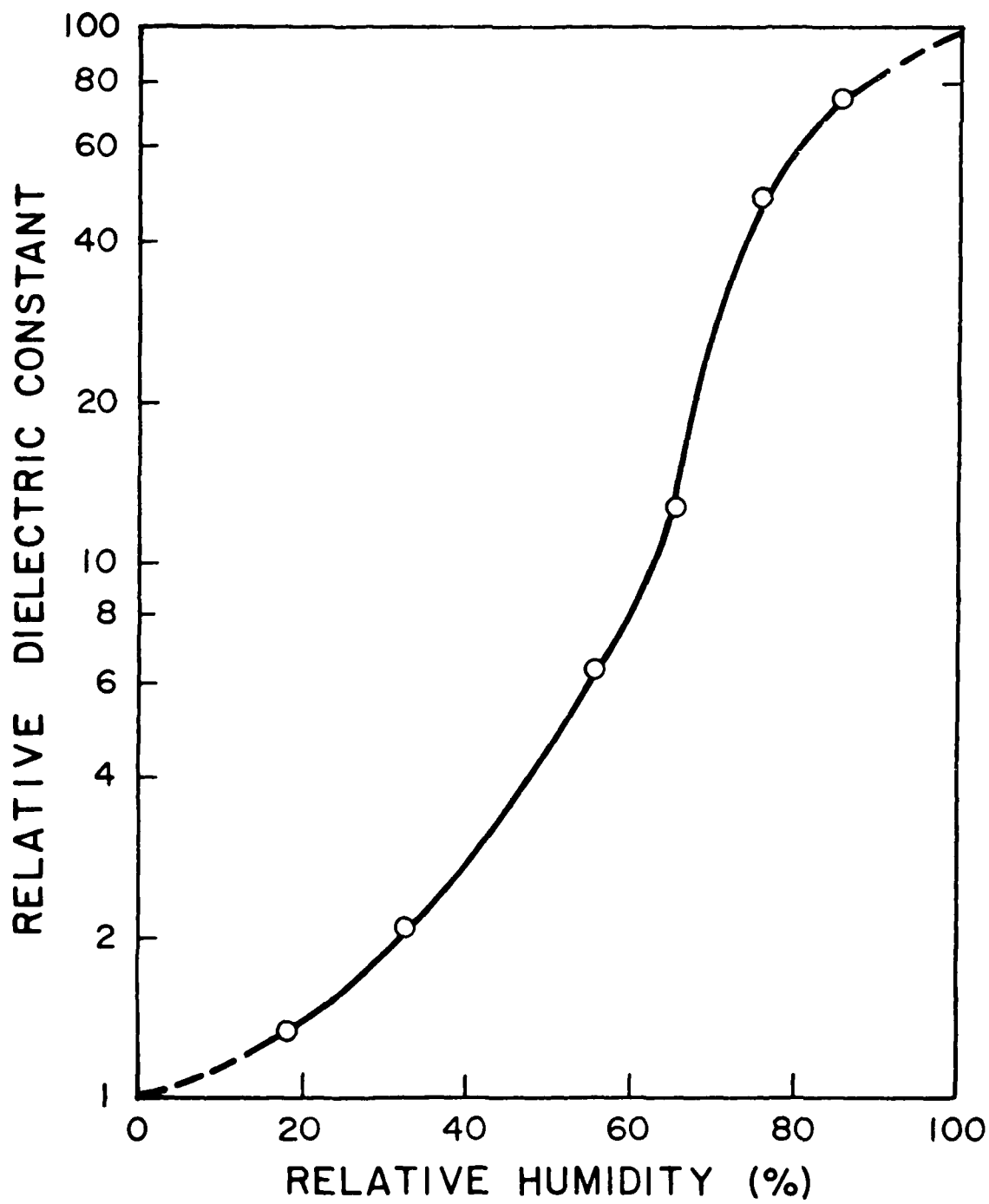
Figure 2.14 The effect of relative humidity on the room temperature
dielectric constant of PbTiO$_3$ films.
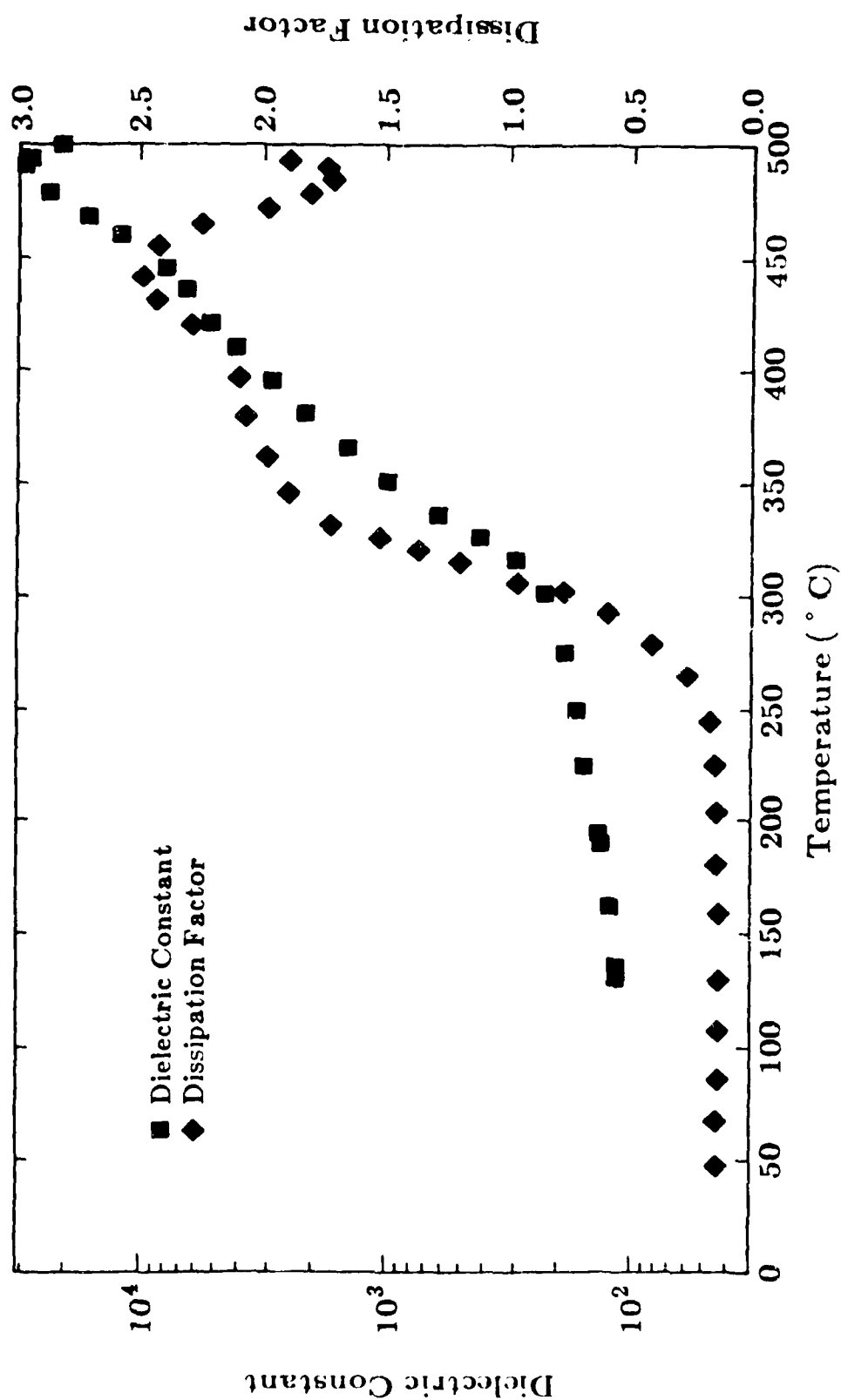
Figure 2.15 The temperature dependence of dielectric constant and dissipation factor for a tetragonal $PbTiO_3$ film 1.83 μm thick.

495°C. The dissipation factor remained almost constant until 250°C and then increased rapidly with further increase in temperature. There was a relative minimum value of dissipation factor around the Curie temperature. The rapid increase of conductivity a few degrees above the Curie temperature made it difficult to measure the dielectric constant and dissipation factor at higher temperatures. Figure 2.16 shows the dielectric constant and dissipation factor changes with temperature for a glass-ceramic (tetragonal plus amorphous $PbTiO_3$) film with six layers, each 305 nm thick. A pseudo-Curie point was observed at 435°C, with K value equal to 2×10^4. Similar to the results shown in Fig. 2.15, the dissipation factor had its relative minimum value at the pseudo-Curie temperature.

Figure 2.17 shows the temperature dependence of dielectric constant and dissipation factor for two samples both having the same thickness and crystal structure (fired with exactly the same temperature profile), but with one of them fired at an applied D.C. field of 8.5 kV/cm. As discussed in Section 2.3.3, the c/a value for the sample fired in the D.C. field will be smaller than that of the one fired without the field. Figure 2.17 indicates that the c/a value has no considerable effect on the dissipation factor in the range 50 ⁻ 450°C, but it does effect the temperature dependence of the dielectric constant. The c/a values of the samples whose temperature dependence of dielectric constant are shown in Fig. 2.17 are 1.057 and 1.055, and it can be seen from Fig. 2.18 [23] that the film with c/a value of 1.055 corresponds to a temperature 30 to 40°C higher than the one with c/a value of 1.057. If the dielectric constant-temperature curve for the sample with c/a = 1.055 in
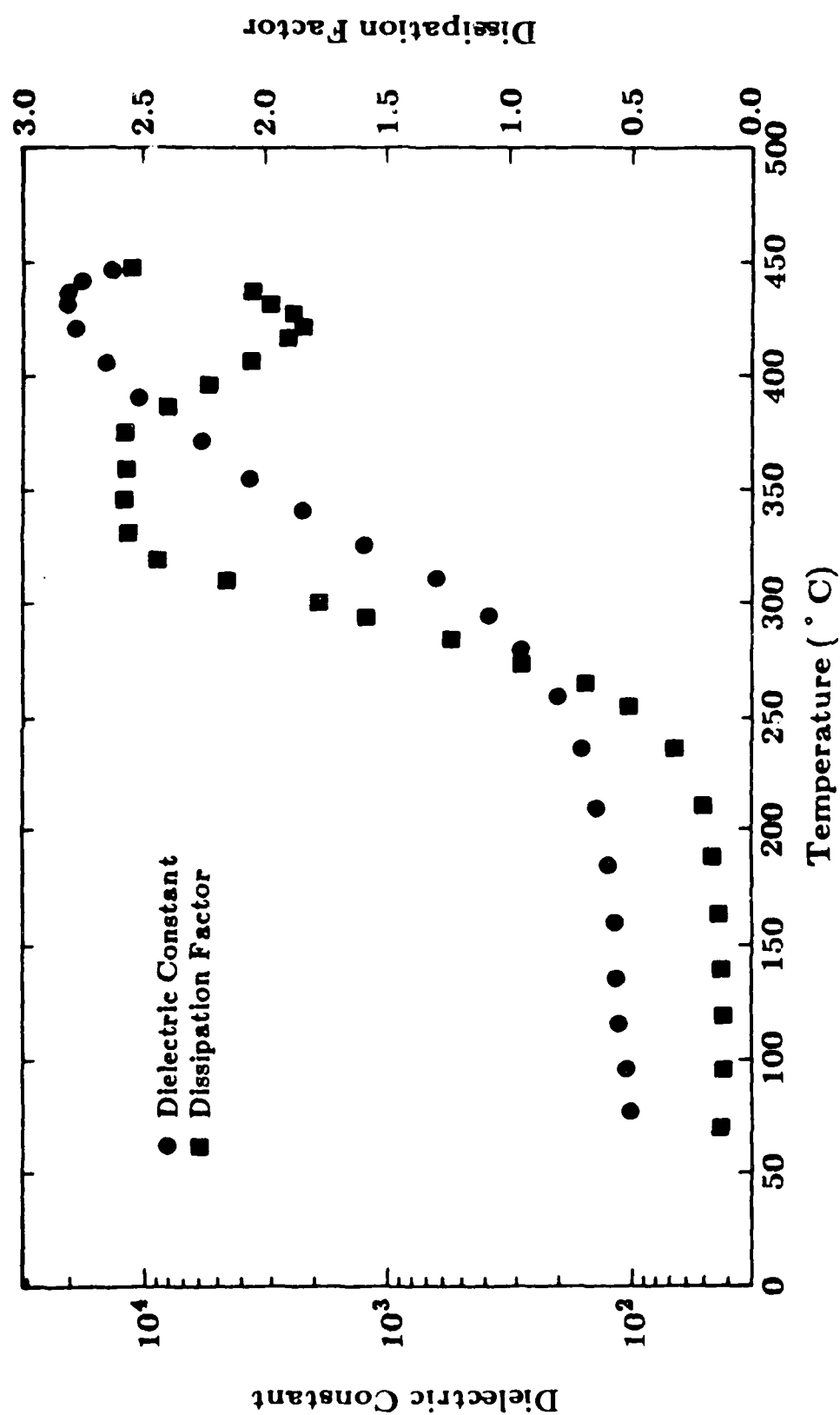
Figure 2.16 The temperature dependence of dielectric constant and dissipation factor for the film composed of tetragonal polycrystalline and amorphous phases.
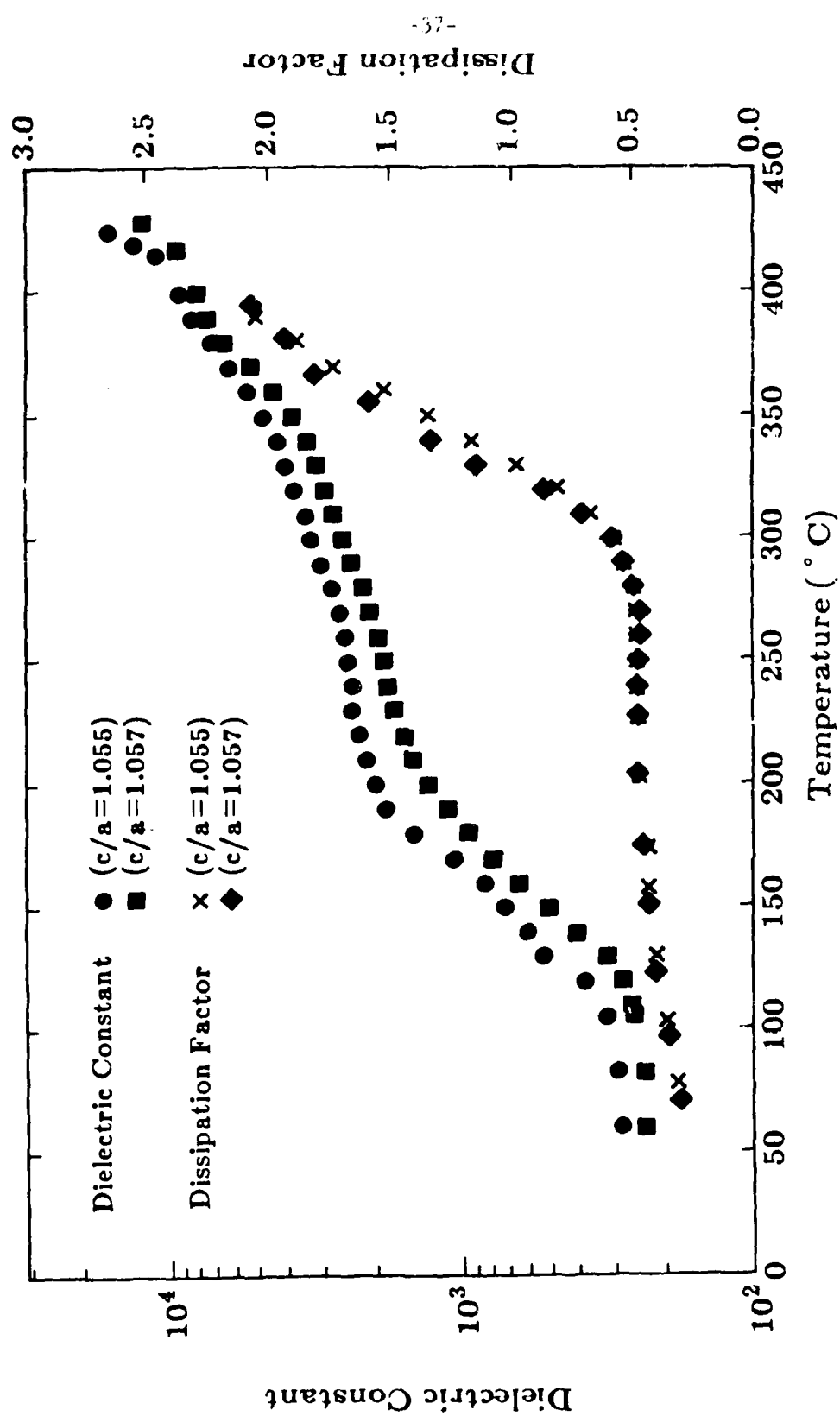
Figure 2.17 The temperature dependence of dielectric constant and dissipation faction for films having some crystal structure but with different values of c/a.
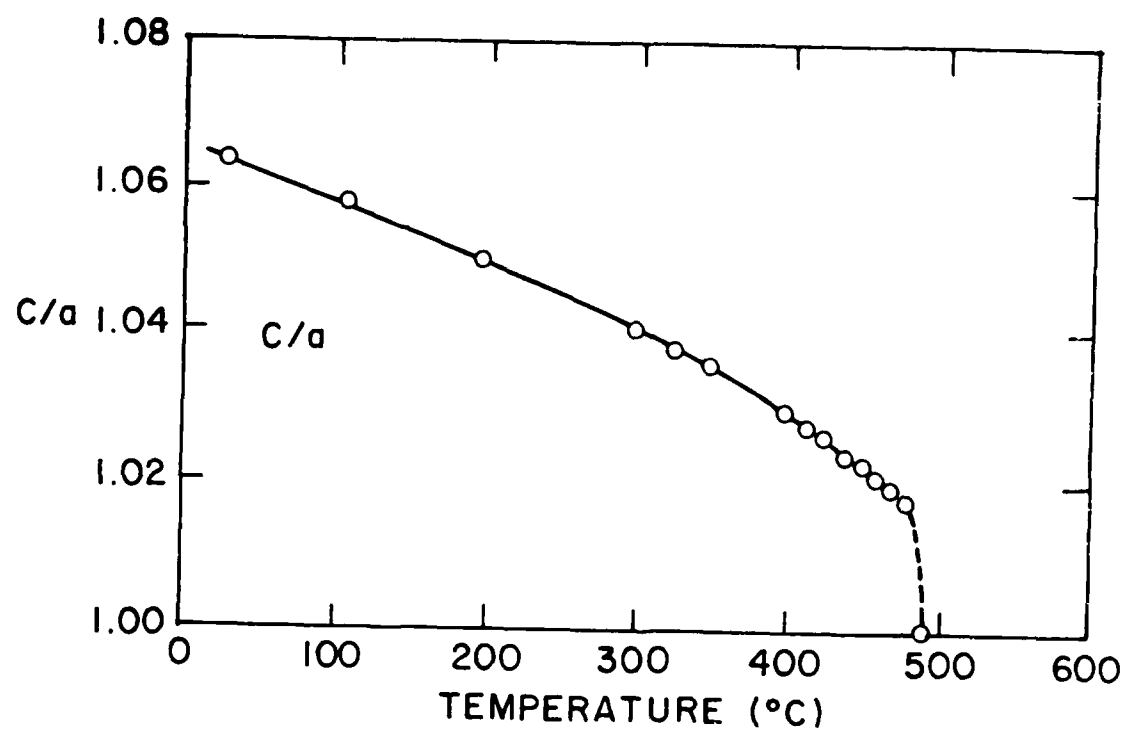
Figure 2.18 Axial ratio of PbTiO_3 as a function.

Figure 2.17 is moved to right about $40^\circ C$, the two curves will match very well over the whole temperature range.

2.3.5.2 D.C. Resistivity

Figure 2.19 shows the temperature dependence of D.C. resistivity for one of polycrystalline films. No effect of film thickness on D.C. resistivity was found. The $\rho - 1/T$ relation is a combination of two almost-straight lines. The change of slope near $250^\circ C$ indicates a change in conductive mechanism. The room temperature resistivity was $1.0 \sim 1.2 \times 10^{10}$ Ω cm, which is comparable to that given in Ref. [25].

2.3.5.3 Spontaneous Polarization

The P-E hysteresis loops were observed for the $PbTiO_3$ films deposited on Pt coating Si wafers, and an example is shown in Fig. 2.20. The spontaneous polarization and remanent polarization under an applied field of 100 kV/cm were about 5.1 $\mu C/cm^2$ and 3.82 $\mu C/cm^2$, respectively. In general, these values were found to be independent of thickness for films with the same phase composition. The coercive field was 33.2 kV/cm. Increasing the applied field beyond 100 kV/cm resulted in the destruction of the top elctrodes (vacuum deposited gold films about 100 nm thick). The dielectric strength for the films grown from the metallo-organic precursors was definitely larger than 100 kV/cm.
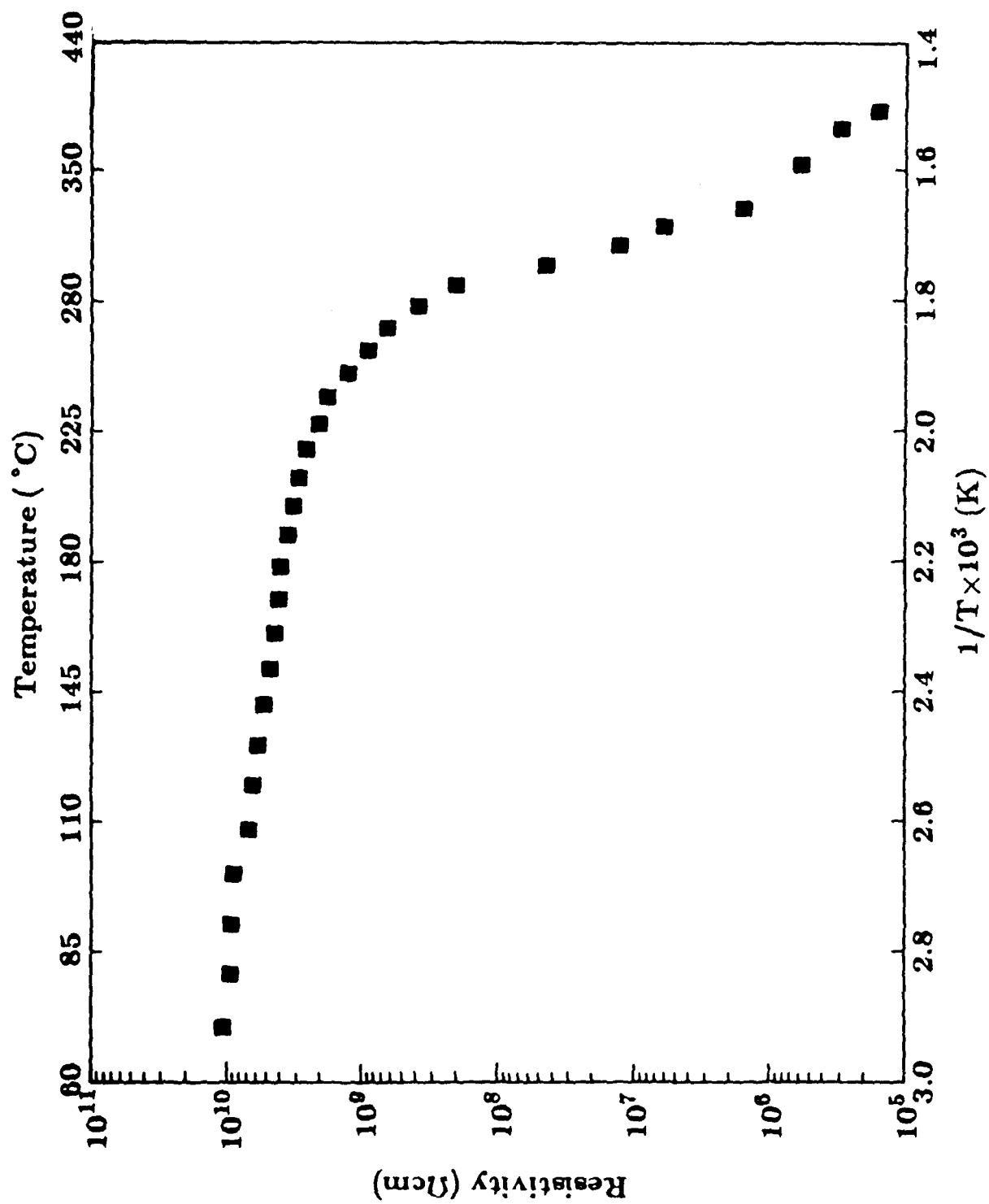
Figure 2.19 The temperature dependence of D.C. resistivity.
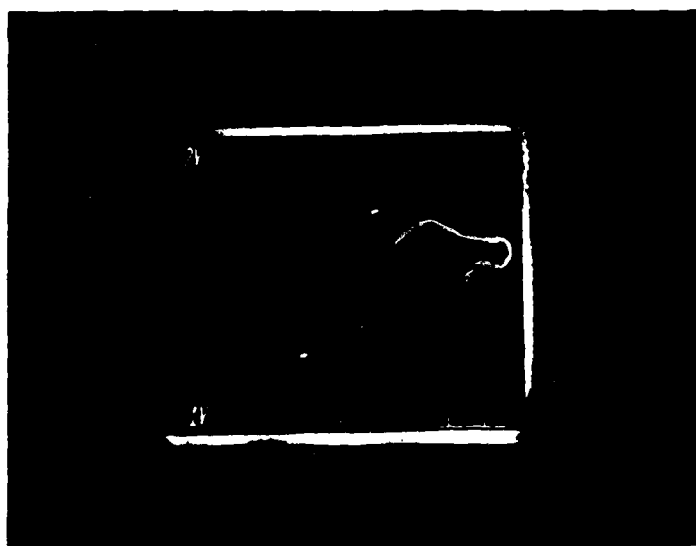
Figure 2.20   Hysteresis loop for PbTiO$_3$ films under an applied
field of 100 Kv/cm (x: 100 Kv/cm/div.,
y: 3.20 μc/cm^2/div.).

2.3.6 Reliability Studies

One of the objectives of this study was to grow thin dielectric films from metallo-organic precursors that were reliable films over an appreciable area. The reliability for the specimens with thickness 0.5 μm to 2 μm was defined as the percent of the planer capacitors (see Fig. 2.1), which gave equivalent dielctric properties with an applied field of 100 kV/cm. The reliability of the specimens was found to depend on many factors such as: the choice of substrate; the purity of the metallo-organic precursors; the process cleanliness; and the time-temperature firing profile. For the films made by the multi-layer spinning technique, the reliability was also found to depend on the single layer thickness; Fig. 2.22 shows this relation. Currently, 2 cm X 2 cm dielectric films 0.5 μ to 2.0 μ thick can be made from metallo-organic precursors with 100% reliability using the multilayer technique.

2.4. Summary

Ferroelectric $PbTiO_3$ films with thickness 0.5 μ to 2.0 μ were prepared by the MOD process using a multilayer spinning technique. The processing can yield highly reliable films with easy control of crystal structure and composition at a low firing temperature. Dielectric constants and dissipation factors were measured from $50^{\circ}C$ to $500^{\circ}C$, and the dielectric constant reached 3×10^4 at the Curie temperature of 493-$495^{\circ}C$. The temperature dependence of dielectric constant was found to
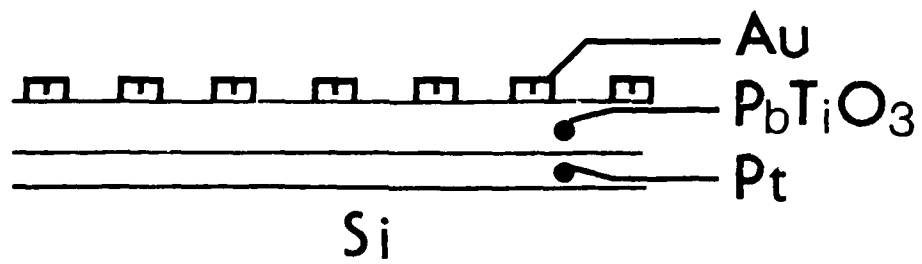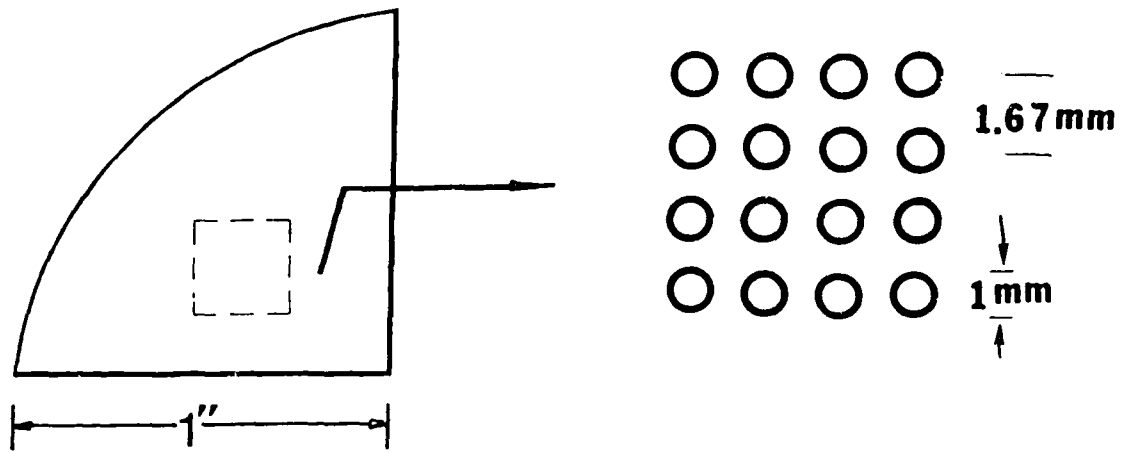
Figure 2.21   An illustration of planer capacitors made by PbTiO$_3$ film.
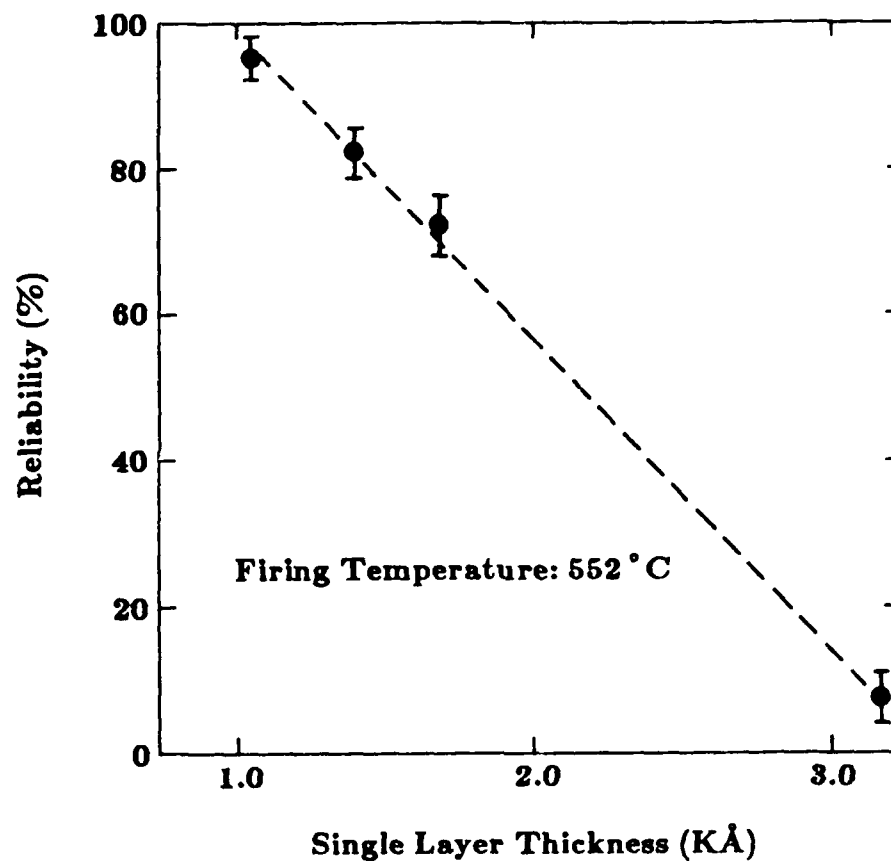
Figure 2.22 The reliability dependence on single layer thickness of
films fired at the same temperature profiles.

be a function of the c/a value, which could be modified by either control of the single layer thickness or the strength of an applied D.C. field during film preparation. The P-E hysteresis loops were measured, and the spontaneous polarization and remanent polarization under an applied field of 100 kV/cm were found to be 5.1 $\mu C/cm^2$ and 3.29 $\mu C/cm^2$, respectively. The dielectric strength for 0.5 ~ 2.0 μ thick films was larger than 100 kV/cm.

The value of c/a for tetragonal polycrystalline films in the range of single layer thickness 75-425 nm was found to be smaller than that of bulk materials. A metastable pyrochlore structure, which formed from amorphous $PbTiO_3$, was observed in the temperature range froom 500 - 550°C. At lower firing temperatures ($<550^o$C), the grain orientation in polycrystalline tetragonal films was random. For firing temperatures higher than 600°C, a strong tendency for preferred orientation with the c axis perpendicular to the substrate surface was observed.

2.5. References

1. F. Jona and G. Shirane, "Ferroelectric Crystals", Pergamon Press, Oxford 1962.

2. V. Bhide, K. Deshmukh and M. Hegde, "Ferroelectric Properties of $PbTiO_3$", Physics 28, 871 (1962).

3. F. Fesenko, V. Gavrilachenko and E. Zarochenehcev, Izv. Akad. Nank. SSS$, 34, 2541 (1970).

4. E. Subbarao, "Studies on Lead Titanate Ceramics Containing Niobium or Tantalum", J. Am. Ceram. Soc., 43, 119 (1960).

5. S. Ikegami. I. Ueda and T. Nagato, "Electrochemical Properties of PbTiO$_3$ Ceramics Containing La and Mn", J. Acoustical Soc. America, 50, 1060 (1971).

6. I. Ueda, "Effects of Additives on Piezoelectric and Related Properties of PbTiO$_3$ Ceramics", Jpn. J. Appl. Phys., 11, 450 (1972).

7. S. Ikegami and I. Ueda, J. Phys. Soc. Japan., 22 725 (1967).

8. Y. Yamashita, K. Yokoyama, H. Honda and T. Takahashi, Jpn. J. Appl. Phys., 20, 183 (1981), Suppl 20-4.

9. Y. Yamashita, S. Yoshida and T. Takahashi, "Effects of MnO Additive on Piezoelectric Properties in Modified (Pb, Ca) TiO$_3$ Ferroelectric Ceramics", Jpn. J. Appl. Phys., 22, 40 (1983), Suppl. 22-2.

10. I. Ueda and S. Ikagami, "Piezoelectric Properties of Modified PbTiO$_3$ Ceramics", Jpn, J. Appl. Phys., 7, 236 (1968).

11. M. Kitabatake, T. Mitsuyu and K. Wasa, "Structure and Electrical Properties of Amorphous PbTiO$_3$ Thin Films Sputtered on Cooled Substrates", J. Non-Crystalline Solids, 53, 1 (1982).

12. M. Okayama, et.al., "Preparation of PbTiO$_3$ Ferroelectric Thin Film by RF Supttering", Jpn. J. Appl. Phys., 18, 1633 (1979).

13. M. Kojima, et.al., "Chemical Vapor Deposition of PbTiO$_3$ Thin Film", Jpn. J. Appl. Phys., 22, 14 (1983).

14. G.M. Vest and R.W. Vest, "A Generic Gold Conductor from Metallo-Organic Compounds", Int. J. Hybrid Microelectronics, 5, 62 (1982).

15. R.W. Vest, et.al., "Ink Jet Printing of Hybrid Circuits", Int. J. Hybrid Microelectronics, 6, 261 (1983).

16. G.M. Vest, et.al., "Metallo-Organic Deomposition (MOD) Films for Electronic Packaging", Proceedings of Materials Research Society Symposium G, Palo Alto, CA, April (1986).

17. C. Sabo, et.al., "Silver Thick Film Metallization for Photovoltaics Fired at $300^{o}C$", Proceedings of the International Society for Hybrid Microelectronics symposium, Anaheim, CA, No. 1985, p. 59.

18. G.M. Vest and S. Singaram, "Synthesis of Metallo-Organic Compounds for MOD Powders and Films", Proceeding of Materials Research Society Symposium L, Boston, MA, Dec. (1985).

19. Thermal Expansion V. 13, Edited by Y. Touloukian, Plenum Publishing Co., New York (1970).

20. H. Diamant, K. Orenck and R. Pepinsky, "Bridge for Acurate Measurement of Ferroelectric Hysteresis", Rev. Sci. Instr., 28 [1], 30-33 (1957).

21. F. Martin, "A Metastable Cubic Form of Lead Titanate Observed in Titania Nucleated Glass Ceramics", Phys. Chem. of Glass, 6, 143 (1965).

22. International Tables for Cyrstallography, V. 4, No. 227.

23. G. Shirane and S. Hoshino, "On the Phase Transition in Lead Titanate", J. Phys. Soc., Jpn., 6, 265 (1951)

24. A.S. Shaikh and G.M. Vest, "Kinetics of BaTiO$_3$ and PbTiO$_3$ Formation from Metallo-Organic Precursors", J. Am. Ceram. Soc. (accepted).

25. V. Gavrilyachenko, et.al., "Spontaneous Polarization and Coercive Field of Lead Titanate", Sov. Phys. Solid State, 12, 1203 (1970).

3. GRAIN SIZE EFFECTS IN BaTiO$_3$

3.1 General

The room temperature relative permittivities of a single crystal of BaTiO$_3$ are 3400 along the a axis and 150 along the c axis [1]. However, Kniepkamp and Heywang [2] reported a relative permittivity value of 3500 for a polycrystalline, 1 μm grain size BaTiO$_3$. Many other researchers have also reported similar or higher values [3-9]. Keizer and Burggraaf [10] observed similar effects of grain size on the permittivity and the Curie temperature of lanthina substituted lead titanate.

Very high permittivity values observed in fine grained ceramic can not be explained by an averaging procedure. Various explanations have been offered for the grain size dependence of dielectric constant [11-16]. However, none of these theories can explain the sharp decrease of dielectric constant below a certain grain size. The sharp decrease of dielectric constant with decrease in grain size, below 10 nm, was explained by V.P. Dudkevich et al.[17] and Srinivasan et al. [18] using

the Lyddane-Sachs-Teller relationship. However, this effect is insignificant for the grain sizes higher than 10 nm. The dielectric constant of powdered $BaTiO_3$ was observed to be very low by various researchers [19-21]. Goswami [20] attributed the lower dielectric constant to a surface defect layer.

3.2 Experimental

Barium titanate powder was obtained by decomposition of metalloorganic compounds using the procedure outlined elsewhere[22]. Approximately 0.15 g of $BaTiO_3$ powder was pressed at about 550 MPa to obtain disk shaped pellets (diameter ~6 mm, thickness ~1.25 mm). The pellets were placed on a bed of powder of the same composition in a platinum crucible and fired at temperatures ranging from $1050^{\circ}C$ to $1300^{\circ}C$, for 5 to 30 minutes. The grain sizes of the thermally etched samples were determined using SEM[+]. The grain sizes and densities of such samples are listed in Table 3.1. The sintered pellets were painted with a Pd-Ag thick film conductor composition[++], dried at $200^{\circ}C$ and fired at $850^{\circ}C$ for about 15 minutes. Thin gauge copper wires were soldered to both sides of the samples. To avoid the effects of condensed moisture, the samples were sprayed with a protective coating[+++]. Anomalous electrical properties were observed at the dew point if the coating was not used.

+ JEM/200CX JOEL Inc., Peabody, MA

++ No. 6120, DuPont Inc., Niagara Falls, N.Y.

+++ Crystal Clear,No. 1302, Borden Inc., Columbus, OH.

Table 3.1 Density and grain size of BaTiO$_3$ ceramics.

Time min.	Tempearture $^\circ$C	Grain size μm	Density % theoretical
30	1050	0.3	58
30	1100	0.35	62
30	1150	0.4	64
30	1200	0.5	66
30	1225	2.8	78
05	1300	9.6	74
30	1300	15.5	79

The dielectric properties of the samples were measured as a function of temperature. An environmental chamber[++++] was used to vary the temperature of the sample in air from $-70^{\circ}C$ to $+160^{\circ}C$. The temperature of the specimens was measured with an alumel-chromel thermocouple.

The dielectric constant and the dissipation factor of the specimens were measured using a digital LCR meter[#]. All the dielectric properties were measured at 1 kHz test frequency, and using zero D. C. bias and 1 Vrms test signal. Spontaneous polarization measurements were carried out using the hysteresis loop bridge circuit suggested by Diamant et al. [23].

3.3 Results and Discussion

3.3.1 Experimental Results

Since $BaTiO_3$ can be produced at considerably lower temperature by the MOD process, very fine particle size $BaTiO_3$ can be obtained. The crystallite size of $BaTiO_3$ powder obtained at $850^{\circ}C$ was 0.045 μm. This powder was pressed into pellets and sintered under the conditions listed in Table 3.1. The microstructure of the sintered pellets was studied using the SEM. All the samples fired below $1300^{0}C$ showed a relatively uniform grain size, and the average grain size of each was calculated by Hilliard's method [24]. The samples fired at $1300^{\circ}C$ had a bimodal grain size distribution, and the average grain size was calculated using arithmetic average procedures. The porosity of the samples ranged from

++++ Model SK 2101,Associated Testing Laboratories Inc., Wayne, NJ.

 # No. 4262A Hewlett Packard Inc., Palo Alto, CA.

56 to 80% as determined by geometry. Since the samples were not 100 %
dense, the measured dielectric constants were corrected for porosity.
Numerous formulae have been suggested for the dielectric constant of a
heterogeneous system in terms of the dielectric constant and volume
fraction of the individual phases [25]. In the present case, the dielec-
tric constants were corrected for porosity using effective medium theory
[26] for coordination number 6. Figure 3.1 shows the temperature
dependence of the corrected dielectric constant of the various samples
with differing grain sizes as a function of temperature. As the grain
size decreased, the cubic-tetragonal transition temperature decreased by
about $2-4^{o}C$ and the tetragonal-orthorhombic transformation temperature
increased considerably. To avoid the effect of transition temperature
on the isothermal dielectric constant, the dielectric constant at $70^{0}C$
was plotted as a function of grain size as shown in Fig. 3.2. As the
grain size of $BaTiO_3$ increased, the dielectric constant increased,
reached a maximum at about 0.4 μm and then decreased with further
increase in grain size. A similar behavior was observed by Brandmayr
[7], K. Kinoshita and A. Yamaji [9] and G. Arlt et al. [8]. However,
Brandmayr and K. Kinoshita and A. Yamaji observed the maxima at about
1.0 μm and Arlt et al. at 0.7 μm.

3.3.2. Model

A maximum in the dielectric constant indicates that there are
opposing factors which influence the grain size dependence of the
dielectric constant. Grain boundaries are amorphous in nature, and
hence have a lower dielectric constant than the grains. Since the
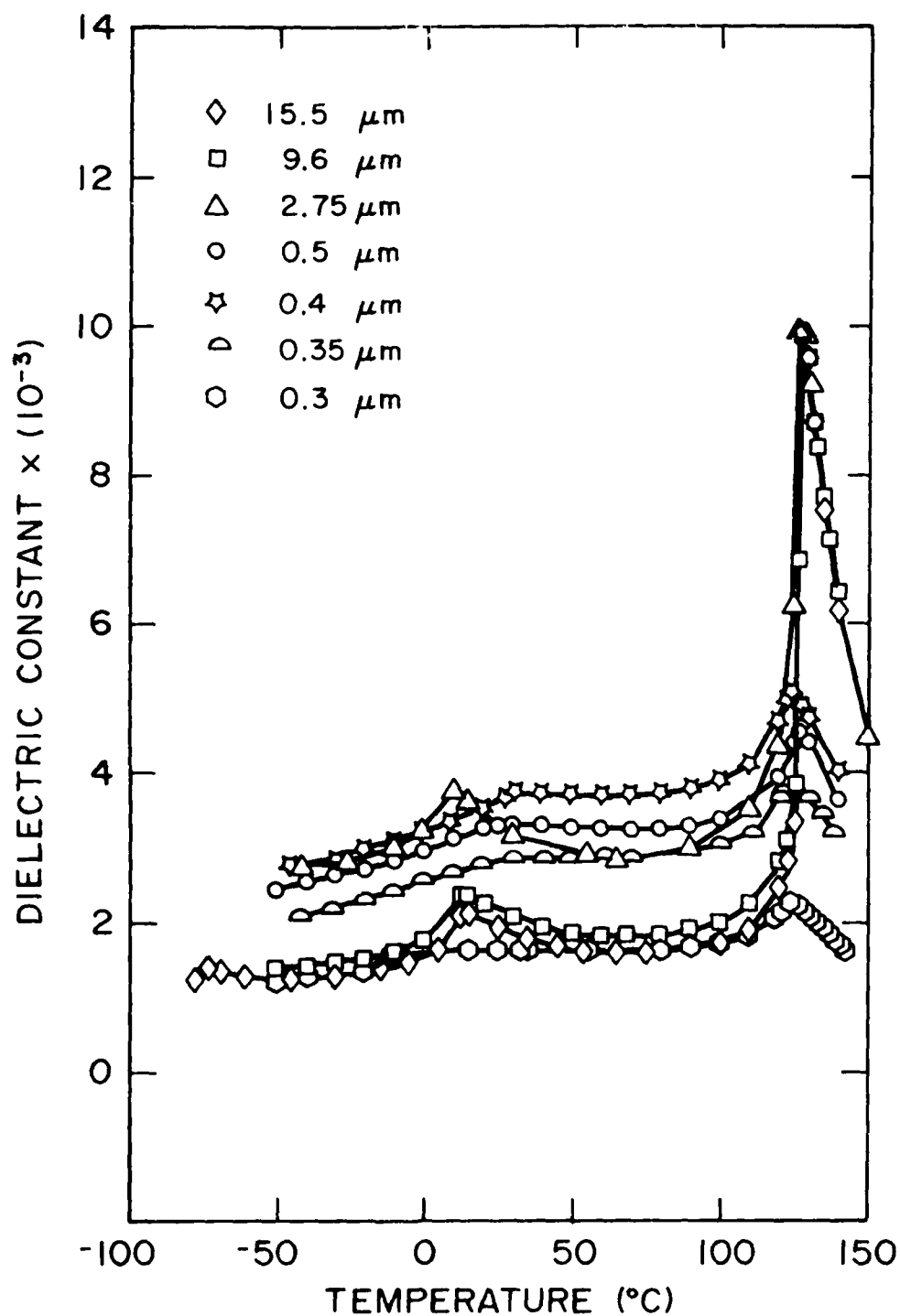
Figure 3.1 Variation of dielectric constant of BaTiO$_3$ ceramics
of varying grain sizes with temperature.
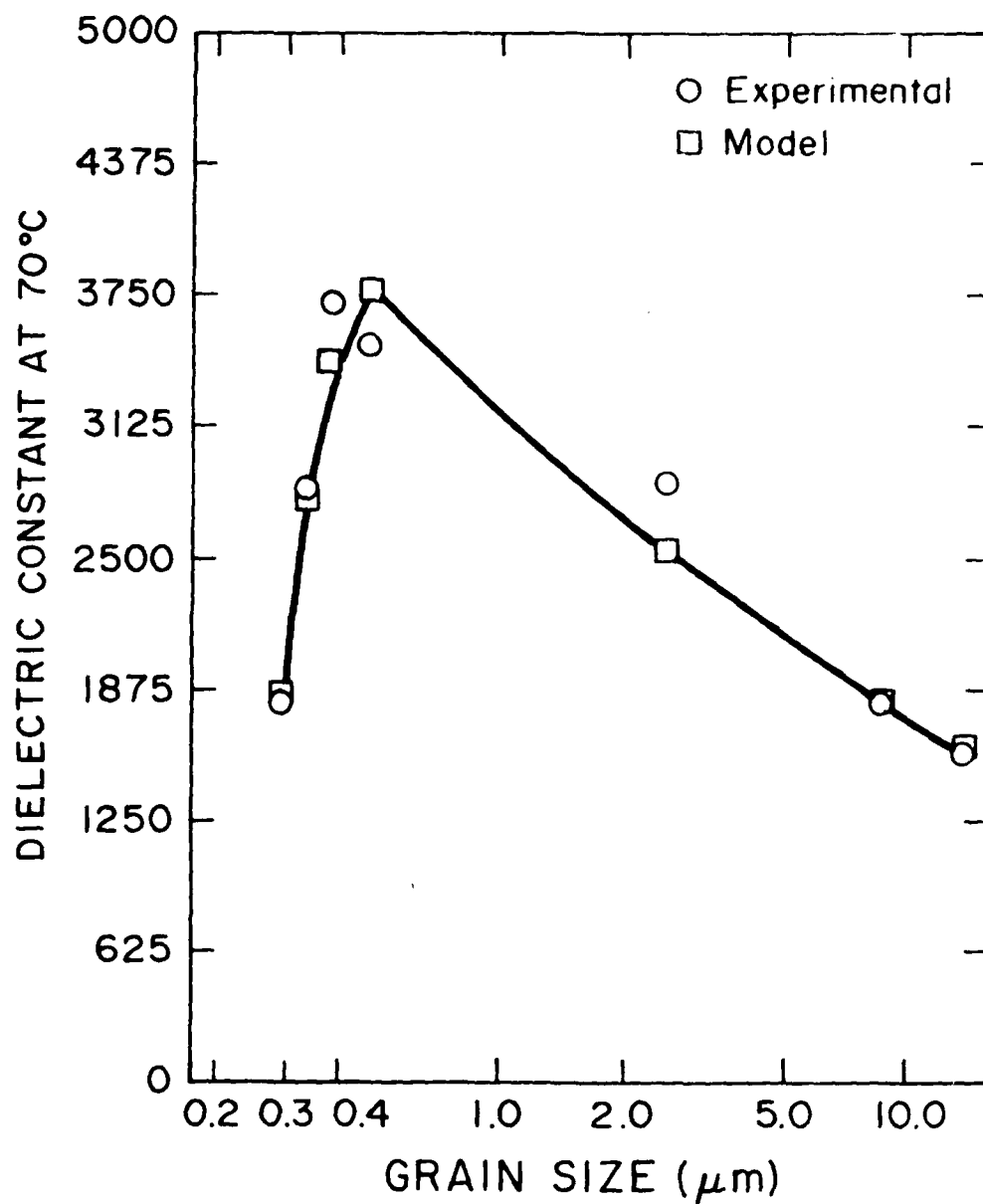
Figure 3.2 A comparison of experimental behavior of dielectric constant with grain size and the one predicted by model.

fraction of grain boundary volume increases with decreasing grain size, the dielectric constant of polycrystalline $BaTiO_3$ should decrease with decreasing grain size. On the contrary, the contribution of internal stresses [11], internal electric field [12] and domain wall area [8], all of which increase the dielectric constant, increase with decreasing grain size.

The model used to calculate the dielectric constant of the system is shown in Fig. 3.3. Figure 3.3 shows an array of cubic grains surrounded by grain boundaries, which can be represented by a series and parallel combination of grain and grain boundary dielectrics. The total dielectric constant of a grain is made up of intrinsic dielectric constant which results from ferroelectric phenomenon and is affected by external factors such as electric field and stresses, and the extrinsic dielectric constant which results from domain wall motion etc. In this model, the following simplifying assumptions were made.

3.3.3 Assumptions

1. Grains are cubic.

2. Grain boundaries have a low dielectric constant.

   The dielectric constants of the surface defect layers observed in the

   single crystals or polycrystalline powders are in the range of 5 to

   200 [27-29].

3. Thickness of the grain boundaries follows a relation,
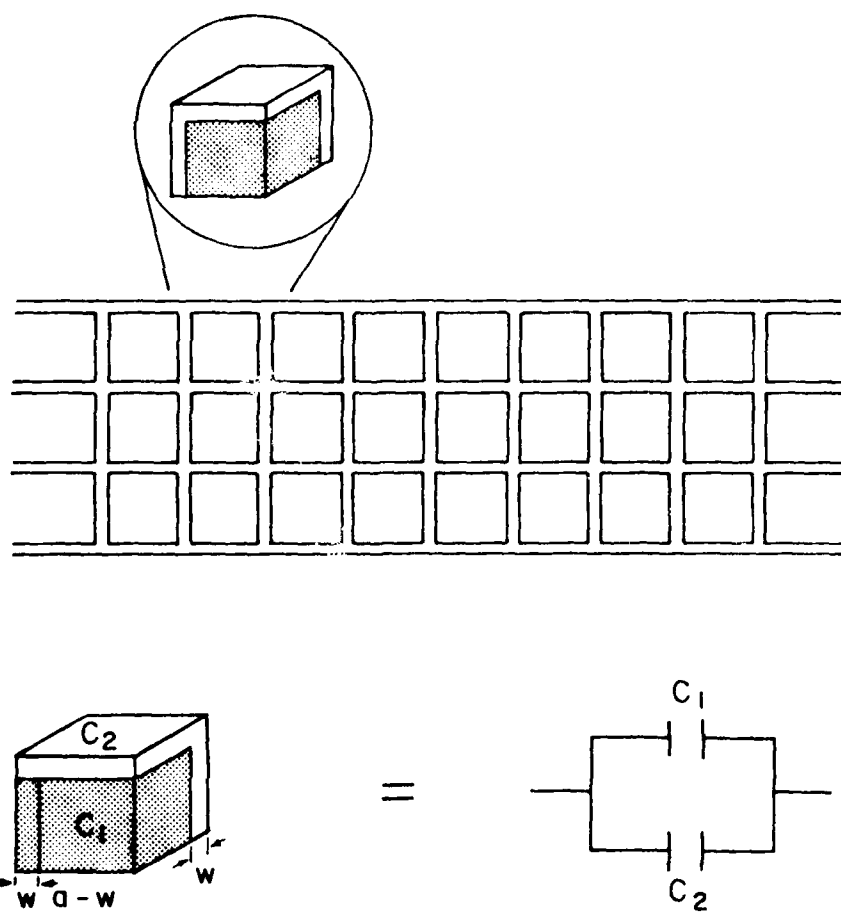
Figure 3.3 A schematic of the proposed model.

$$w = \frac{1}{(D_o exp(-Q/RT)*t)^{0.5}} \qquad (1)$$

where, w=thickness, D_o=constant, Q=activation energy, R=gas constant

t=sintering time and T=sintering temperature

This assumes that the boundary thickness is diffusion controlled

and is determined by the sintering conditions.

4. The grains having grain size smaller than 0.4 μm are single domain

grains. This assumption is made based on Arlt et al.'s[8] study.

5. The transformation stresses are experienced only by single domain

grains. The stresses caused by the cubic-tetragonal transformation

are completely relieved by formation of 90° domain in

multidomain grains.

6. The transformation stresses are constant with respect to grain size,

for grain size below 0.4 μm.

7. There is no depolarizing electric field.

8. The dielectric constants of the porous bodies are corrected by

effective medium theory to obtain the dielectric constants of the

dense bodies.

3.3.4. Methodology

The following approach was used to calculate the dielectric constant of polycrystalline material; cgs units are used, as they are more convenient. The dielectric constants of the single crystal under a stress system was calculated using Devonshire's theory [30-31] as follows.

The elastic Gibb's free energy function can be written in terms of stresses and polarization [11] as follows.

$$G1 = -1/2s_{11}(X_x^2 + Y_y^2 + Z_z^2) - s_{12}(X_x Y_y + Y_y Z_z + Z_z X_x)$$

$$-1/2s_{44}(X_y^2 + Y_z^2 + Z_x^2) + (Q_{11}X_x + Q_{12}Y_y + Q_{12}Z_z)P_x^2$$

$$+(Q_{12}X_x + Q_{11}Y_y + Q_{12}Z_z)P_y^2 + (Q_{12}X_x + Q_{12}Y_y + Q_{11}Z_z)P_z^2$$

$$+ Q_{44}(X_y P_x P_y + Y_z P_y P_z + Z_x P_z P_x) + A(P_x^2 + P_y^2 + P_z^2)$$

$$+ B(P_x^4 + P_y^4 + P_z^4) + C(P_x^6 + P_y^6 + P_z^6)$$

$$+D(P_x^2 P_y^2 + P_y^2 P_z^2 + P_z^2 P_x^2)$$

$$+G(P_x^2 P_y^4 + P_x^4 P_y^2 + P_y^2 P_z^4 + P_y^4 P_z^2 + P_z^2 P_x^4 + P_z^4 P_x^2) \qquad (2)$$

where X_x, Y_y, Z_z are the normal stress components,

Y_z, Z_x, X_y are the shear stress components,

s_{11}, s_{12}, s_{44} are the elastic moduli,

P_x, P_y, P_z are the components of polarization,

Q_{11}, Q_{12}, Q_{44} are the electrostrictive coefficients,

A, B, C, D and G are the coefficients of the energy functions.

The coefficients A, B, C, D and G are given by the following expressions [32].

$$A = 3.7*10^{-5}(T - \theta) \tag{2}$$

where T is the experimental temperature and θ is the temperature at which the inverse susceptibility is extrapolated to zero. The present inverse susceptibility studies on the coarse grained $BaTiO_3$ gave the value of θ to be $118^{\circ}C$.

$$B = - \left| \frac{\pi/\varepsilon_c + 2A}{2P_s^2} \right| \tag{4}$$

where ε_c is the dielectric constant along the c axis and P_s is the spontaneous polarization.

$$C = \frac{\pi/\varepsilon_c + A}{3P_s^4} \tag{5}$$

$$D = \frac{1}{P_o^2} \left| A(3\alpha^2 - 4) + B(3\alpha^2 P_T^2 - 2P_o^2) + C(3\alpha^2 P_T^4) \right| \tag{6}$$

where P_o is the polarization in the orthorhombic phase(at the second transformation temperature)= 8×10^4 cgs units, P_T is the polarization in the tetragonal phase (at the second transformation temperature)= 6.5 $\times 10^4$ cgs units

and $\alpha = P_T/P_o = 1.23$

$$G = - \frac{1}{P_o^4} \left| A(\alpha^2 - 1) + B(\alpha^2 P_T^2) + C(\alpha^2 P_T^4 + P_o^4) \right| \qquad (7)$$

Previously [11,32-34], the coefficients A, B, C, D and G were calculated using dielectric constants of flux grown single crystals. Flux grown crystals have $\bar{F}$ as an impurity, and the Curie temperature of such crystals was 120^oC. Melt grown crystals are more pure and have 130 +/- 2 as the Curie temperature. Since, in the present studies the observed Curie temperatures were in the neighborhood of 128^oC, the reported [1] dielectric constants of melt grown crystals were used to calculate the values of the coefficients. Table 3.2 lists the values of the coefficients obtained along with the values of elastic and electrostrictive constants used in the free energy function.

Differentiating Eq.(2) w.r.t. P_s, under the conditions that $P_1 = P_2 = 0$ and $P_3 = P_s$, and under uniform compressive stress X along the c axis and equal tensile stresses -X along the a axes, the following expressions for dielectric constants are obtained. According to assumption 5, X=0 for grain size >0.4 μm.

$$\frac{4\pi}{\varepsilon_c} = 2(Q_{11}X - 2Q_{12}X) + 2A + 12BP_s^2 + 30CP_s^4 \qquad (8)$$

$$\frac{4\pi}{\varepsilon_a} = -2Q_{11}X + 2A + 2DP_s^2 + 2GP_s^4 \qquad (9)$$

$$E_c = 2P_sX(Q_{11} - 2Q_{12}) + 2AP_s + 4BP_s^3 + 6CP_s^5 = 0 \qquad (10)$$

Table 3.2 Values of the coefficients of Devonshire's free energy
function at 70°C.

Coefficient	Reference	Value in CGS units
A	[51]*	$3.7 \times 10^{-5}(T-118)$
B	[51]*	-1.1972×10^{-22}
C	[51]*	1.5502×10^{-22}
D	[51]*	6.0×10^{-13}
G	[51]*	5.0×10^{-23}
Q_{11}	[118]	1.23×10^{-12}
Q_{12}	[118]	-0.48×10^{-12}

* Modified using melt grown single crystal data.

Equation (10) can be solved for P_s to give

$$P_s^2 = \frac{-B + \sqrt{B^2 - 3C(X(-2q_{12} + q_{11}) + A)}}{3C} \qquad (11)$$

Using the value of P_s^2 obtained from Eq. (11) in Eq. (8) and Eq. (9), the values of ε_c and ε_a can be calculated at any stress level. The calculated values of dielectric constants ε_c and ε_a at stress, $X=0$, were 180 and 1850, respectively. The experimental values of dielectric constants ε_c and ε_a of stress free $BaTiO_3$ single crystal, reported by Wemple et. al.[1], were 180 and 1850, respectively.

G. Arlt [8] proposed a method of calculating the dielectric constant of a grain containing domains. The dielectric constant tensor for a grain containing domains is given by

$$\begin{vmatrix} \varepsilon_{11} & 0 & 0 \\ 0 & \varepsilon_{22} & 0 \\ 0 & 0 & \varepsilon_{33} \end{vmatrix}$$

$$(12)$$

where

$$\varepsilon_{11} = \frac{1}{3} \left| \frac{-16\varepsilon_c^4 + 49\varepsilon_c^3\varepsilon_a + 526\varepsilon_c^2 + 405\varepsilon_c\varepsilon_a^3}{9(\varepsilon_c + \varepsilon_a)(2\varepsilon_c^2 + 11\varepsilon_c\varepsilon_a + 5\varepsilon_a^2)} \right| \qquad (13)$$

$$\varepsilon_{22} = \frac{1}{3} \left| \frac{2\varepsilon_c^2 + 11\varepsilon_c\varepsilon_a + 5\varepsilon_a^2}{3(\varepsilon_c + \varepsilon_a)} \right| \qquad (14)$$

$$\varepsilon_{33} = \frac{1}{3} \left| \frac{146\varepsilon_c^3\varepsilon_a + 405\varepsilon_c^2\varepsilon_a^2 + 324\varepsilon_c\varepsilon_a^3 + 81\varepsilon_a^4}{9(\varepsilon_c + \varepsilon_a)(2\varepsilon_c^2 + 11\varepsilon_c\varepsilon_a + 5\varepsilon_a^2)} \right| \tag{15}$$

The dielectric constant of the ceramic was calculated using Bruggeman's [35] formula

$$\varepsilon_r = \frac{1}{4}(\varepsilon_{22} + \sqrt{\varepsilon_{22}^2 + 8\varepsilon_{11}\varepsilon_{22}}) \tag{16}$$

where ε_{22} in Eq. (16) is taken as a average of ε_{22} and ε_{33} given by Eq.(14) and (15) respectively. For a single domain grain $\varepsilon_{11} = \varepsilon_c$ and $\varepsilon_{22} = \varepsilon_{33} = \varepsilon_a$.

According to the assumptions made above, the total dielectric constant of the ceramic should be the result of the intrinsic dielectric constant, the grain boundary effects and the domain wall contribution for the grain sizes above 0.4 microns. For the grain sizes below 0.4 μm, the grains are single domain grains; hence the domain wall contribution is absent. However, the intrinsic dielectric constant is affected by the residual transformation stresses below 0.4 μm.

The domain wall contribution to the dielectric constant was calculated using G. Arlt's[08] method.

$$\varepsilon_{dw} \propto \text{domain wall area(A)} \tag{17}$$

ε_{dw} is domain wall contribution to the dielectric constant.

$$A \propto 1/d \tag{18}$$

d is domain width. Thus,

$$\varepsilon_{dw} = \frac{k}{d} \tag{19}$$

G. Arlt [8] related the equilibrium domain size(d) to grain size(a) by the relation

$$d = \sqrt{\frac{128\pi\sigma a}{c_{11}S_s^2}} \tag{20}$$

where c_{11}, S_s and σ are the longitudinal elastic constant, spontaneous deformation and domain wall energy respectively. Therefore, the domain wall contribution to the dielectric constant can be expressed in terms of the grain size by:

$$\varepsilon_{dw} = \frac{K}{\sqrt{a}} \tag{21}$$

Since, at the largest grain size, the internal stresses are completely relieved by formation of 90° domains and the volume fraction of grain boundaries is minimal, the dielectric constant of ceramics of 15.5 μm grain size $(\varepsilon_{15.5})$ was assumed to be the sum of intrinsic and domain wall contributions.

$$\varepsilon_{15.5} = \varepsilon_r + \varepsilon_{dw} \tag{22}$$

ε_r was calculated using Eq. (16) and substracted from the measured value of $\varepsilon_{15.5}$ to obtain the domain wall contribution. Using this, the value of K was calculated from Eq.(21) to be 2710.

The ceramics sketched in Fig. 3.3 can be represented by two capacitors of capacitance C_1 and C_2 in parallel as shown Fig. 3.3. The capa-

citances C_1 and C_2 are given by the following expressions

$$C_1 = \frac{\varepsilon_1 \varepsilon_2 (a - w)^2}{\varepsilon_1 (a - w) + \varepsilon_2 w} \tag{23}$$

$$C_2 = \frac{w(2a - w)}{a} \varepsilon_1 \tag{24}$$

The total capacitance is the sum of C_1 and C_2. Thus, the effective dielectric constant is given by

$$\varepsilon = \frac{w(2a - w)\varepsilon_1}{a^2} + \frac{\varepsilon_1 \varepsilon_2 (a - w)^2}{\varepsilon_1 a(a - w) + \varepsilon_2 aw} \tag{25}$$

where ε_1 is dielectric constant of the grain boundary and ε_2 is the dielectric constant of ceramic calculated using Eqs. (8) through (21).

The thickness of the defective layer "w" is related to the processing conditions through Eq. (1). Using Eqs. (7) through (22) in Eq. (25) leaves the dielectric constant of the grain boundary, D_o, Q and stress as the only unknowns in Eq.(25). The values of these parameters obtained by least square fit using all the data are listed in Table 3.3. The value of "Q" obtained by the least square fit is in good agreement with the value of activation energy obtained in the kinetics of formation of barium titanate studies [22], and the value of the dielectric constant of the grain boundary is in good agreement with the previous studies [27-29]. Using these values, the dielectric constants were calculated at various grain sizes. Figure 3.2 shows the comparison between experimental behavior and the behavior predicted using this model. The experimental observations agree very well with the model.

Table 3.3 Values of the model parameters obtained by least square fit.

Parameter	Value
Dielectric constant of grain boundary	90
Activation Energy (Q) (kJ/mole)	290
D_o ($cm^{-2}.hr^{-1}$)	10^{24}
Stresses ($dynes/cm^2$)	1.26×10^9

The spontaneous polarization is linked to the ferroelectric phenomenon, and hence is related to the intrinsic dielectric constant. As grain size decreases, the crystallanity decreases and finally one reaches an amorphous state where ferroelectricity ceases. Thus, it was expected that the spontaneous polarization should decrease with decrease in grain size. Also, the random orientation of grains makes only a component of spontaneous polarization contribute to the measured value. The expected behavior of spontaneous polarization with respect to grain size was observed, as shown in Fig. 3.4. A linear porosity correction was made to the values of spontaneous polarization in Fig. 3.4.

G. Arlt and Sasko [36] studied the domain structure of polycrystalline BaTiO$_3$. They observed a spatial domain configuration as shown in Fig. 3 5 in unpolarized ceramic, where A=$[01\bar{1}]$, B=$[10\bar{1}]$ and C=$[1\bar{1}\ 0]$ planes. The spontaneous polarization of such a configuration is $P_\alpha = \frac{\sqrt{2}P_s}{3}$, and the vector is directed along $[110]$. Since the grains are randomly oriented in space, the net polarization will be the spatial average of the P_α vector.

$$P_{ceramic} = \int\int_{\frac{\pi}{2}\frac{\pi}{2}}^{\frac{\pi}{2}\frac{\pi}{2}} \frac{P_\alpha \cos\theta \cos\phi \, d\theta d\phi}{\pi^2} \qquad (26)$$

Integration yields $P_{ceramics} = \frac{4\sqrt{2}}{3\pi^2}P_s = 0.19\ P_s$. The value P_s for grain size 15.5 is 0.10 (Coul/m^2) and that for the single crystal BaTiO$_3$ is 0.23 (Coul/m^2). Thus, the value of the spontaneous polarization observed in the ceramic material is greater than the $0.2P_s$ for single crystals.
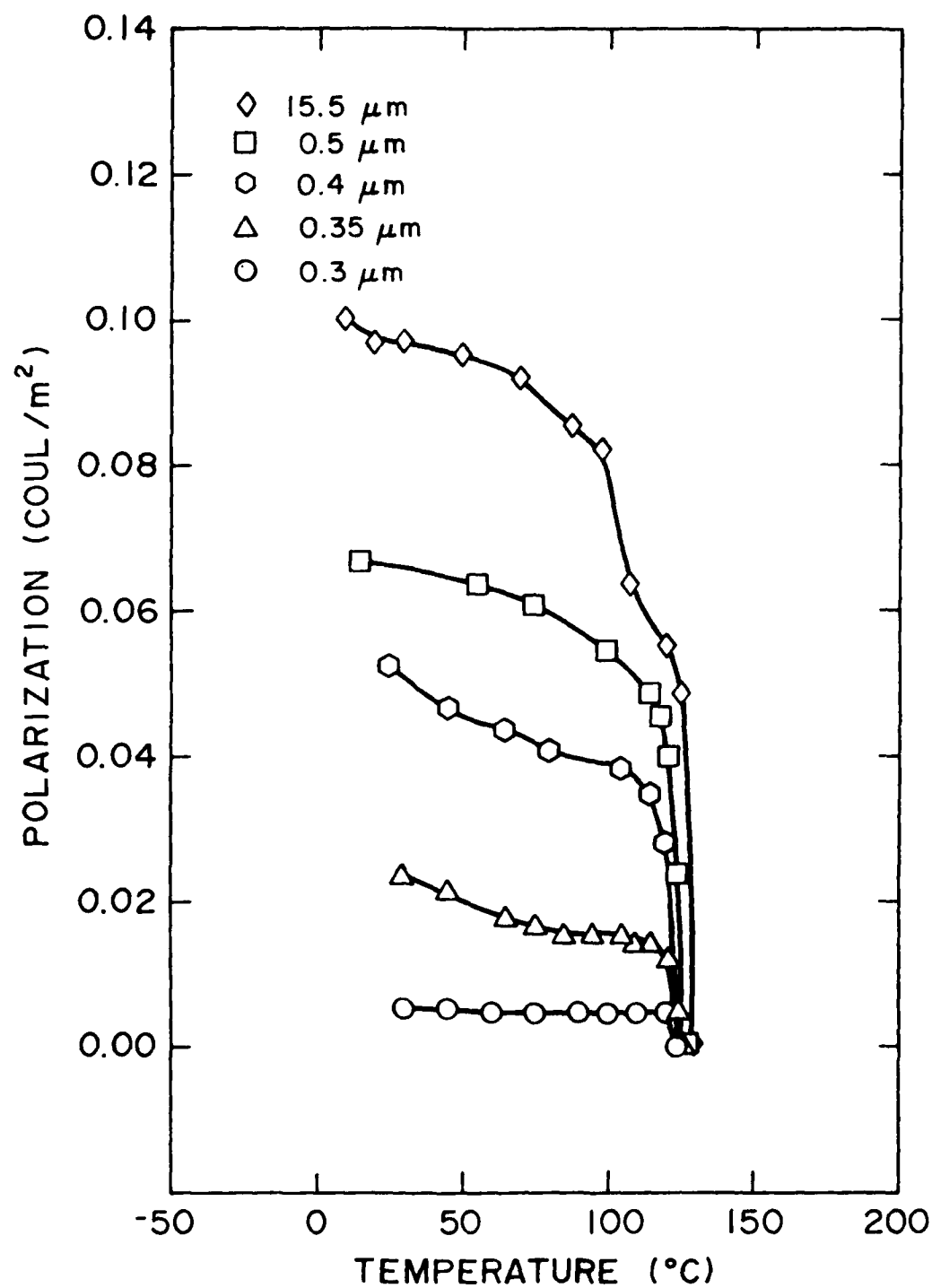
Figure 3.4   Variation of spontaneous polarization of BaTiO$_3$ ceramics of varying grain sizes with temperature.
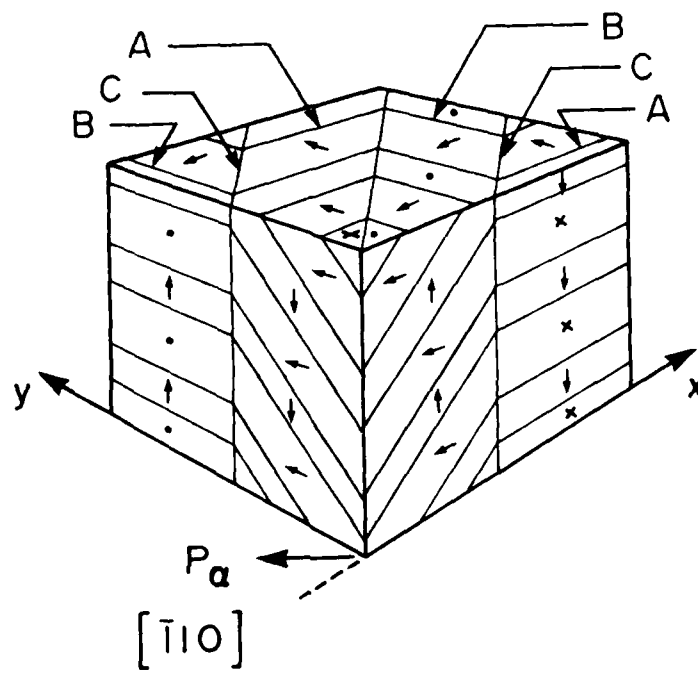
Figure 3.5 α domain configuration observed in unpolarized BaTiO$_3$ ceramics.
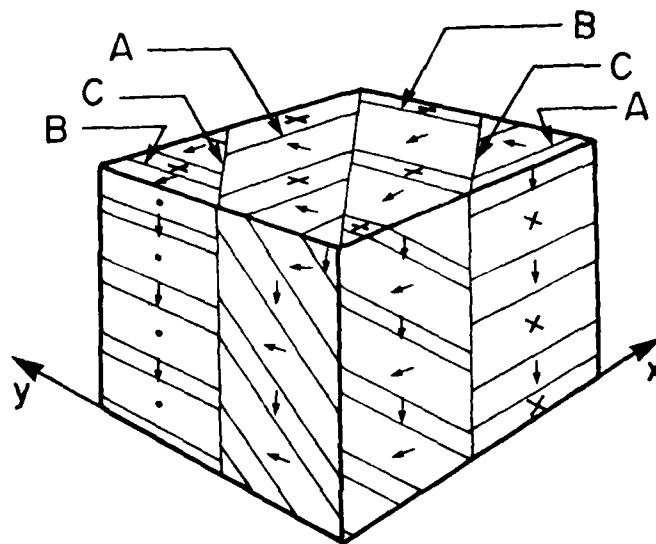
Figure 3.6   A domain configuration observed in polarized BaTiO$_3$ ceramics.

This could be because in polarized ceramics the domain configuration is as shown in Fig. 3.6; this structure has a higher net polarization than the one shown in Fig. 3.5.

3.4   References

1. S. H. Wemple, M. Didomenico,Jr. and I. Camlibel, "Dielectric and Optical Properties of Melt-Grown $BaTiO_3$", J. Phys. Chem. Solids, 29 1797-1803 (1968).

2. H. Kniepkamp and W. Heywang, "Depolarization Effects in Polycry-stalline $BaTiO_3$", Z. Agnew Phys., 6[9] 385-390 (1954).

3. L. Egerton and S. E. Koonce, "Effect of Firing Cycle on Structure and Some Dielectric and Piezoelectric Properties of $BaTiO_3$ Ceramic", J. Am. Ceram. Soc., 38, 412-418 (1955).

4. G. H. Jonker and W. Noorlander; p 285 in Science of Ceramics: vol I. Edited by G. H. Stewart. Academic Press Inc., New York, 1962.

5. A. A. Anaeva et al., "Some Anomalous Properties of Chemically Pure $BaTiO_3$", Bull. Acad. Sci. USSR Phys. Ser.(Engl. Transl.), 24, 1395 (1960).

6. T. M. Herkulich, J. Magder, M. S. Vukasovich and R. J. Lockhart, "Ferroelectrics of Ultrafine Particle Size II: Grain Growth Inhibi-tor Studies", J. Am. Ceram. Soc., 49[6] 295-299 (1966).

7. R. J. Brandmayr, A. E. Brown and Dunlap, "Annealing Effects on Microstructure and Dielectric Properties of Hot Pressed, Ultrafine

Grained $BaTiO_3$", Technical Report ECOM-2614, U.S. Army Electronics Command, Fort Monmouth, N. J., AD622970 (May 1965).

8. G. Arlt D. Hennings and G. de With, "Dielectric Properties of Fine Grained $BaTiO_3$ Ceramics", J. Appl. Phys., 58[4] 1619-1625 (1984).

9. K. Kinoshita and A. Yamaji, "Grain-size Effects on Dielectric Properties in Barium Titanate Ceramics", J. Appl. Phys., 47[1] 371-373 (1976).

10. K. Keizer and A. J. Burggraaf, "Grain Size Effects on the Ferroelectric-Paraelectric Transition, the Lattice Parameters in Lanthana-Substituted Lead Titanate", Phys. Stat. Sol. (a), 26, 561-569 (1974).

11. W. Buessem, A. K. Goswami and L. E. Cross, "Phenomenological Theory of High Permittivity in Fine-Grained Barium Titanate", J. Am. Ceram. Soc., 49[1] 33-36 (1966).

12. A. J. Bell A. J. Moulson and L. E. Cross, "The Effect of Grain Size on the Permittivity of $BaTiO_3$", Ferroelectrics, 54[1-4] 147-150(1984).

13. A. K. Goswami, L. E. Cross and W. R. Buessem, "Internal Field Theory of High Permittivity in Fine- Grained $BaTiO_3$", J. Phys. Soc. Japan, 24[2] 279-281 (1968).

14. H. T. Martirena and J. C. Burfoot, "Grain Size Effects on the Properties of Some Ferroelectric Ceramics", J. Phys. C: Solid State Phys., 7[17] 3182-3192 (1974).

15. H. T. Martrena, Ph. D. Thesis, University of London (1973).

16. H. Heydrich and U. Knaur, "Grain Boundary Effects in Ferroelectric $BaTiO_3$", Ferroelectrics, 31[3/4] 151-156 (1981).

17. V. P. Dudkevich, VI. M. Mukhortov, Yu. I. Golovko, V. A. Bukreev, Vas. M. Mukhortov, Yu. G. Sindeev and E. G. Fesenko, " Dependence of Dielectric Properties of Condensed $BaTiO_3$ Films on the Size of Coherent Scattering Regions", Sov. Phys. Solid State, 23[2] 347-348 (1981).

18. M. R. Srinivasn, M. S. Multani, P. Ayyub and R. Vijayaraghavan, "Soft Modes and Grain Size Effects in Ferroelectric Ceramics", Ferroelectric, 51[1/2] 137-141 (1983).

19. J. Paletto, G. Grange, R. Goutte and L. Eyraud, "A Study of Dielectric Properties of Powdered $BaTiO_3$", J. Phys. D:Appl. Phys. 7[1] 78-84 (1974).

20. A. K. Goswami, "Dielectric Properties of Unsintered Barium Titanate", J. Appl. Phys., 10[2] 619-624 (1969).

21. A. L. Khodakov, "Dielectric Properties of Finely Dispersed Barium Titanate", Fizika Tverdogo Tela(English Translation), 2[9] 1904-1907 (1960).

22. A. S. Shaikh and G. M. Vest, "Kinetics of $BaTiO_3$ and $PbTiO_3$ Formation from Metallo-organic Precursors2", J. Amr. Ceram. Soc., 1986.

23. H. Diamant, K. Drenck and R Pepinsky, "Bridge for Accurate Measurement of Ferroelectric Hysteresis", The Review of Scientific

Instruments, 28[1] 30-33 (1957).

24. J. E. Hilliard, "Estimating Grain Size by the Intercept Method", Metal Progress, 91, 99-102 (May 1964).

25. L. K. H. Van Beek, "Dielectric Behavior of Heterogeneous Systems",pp 69-114 in Progress in Dielectrics Vol 7; edited by J. B. Birks, CRC press, Cleveland Ohio (1967).

26. S. Kirkpatrick, "Classical Transport in Disordered Media: Scaling and Effective Medium Theories", Physical Review Letters, 27[25] 1722-1725 (1971).

27. W. J. Merz, "Switching Time in Barium Titanate and Its Dependence on Crystal Thickness", J. Appl. Phys. 27[8] 938-943 (1965).

28. P. Coufova and H. Arend,"The Thickness Dependence of the Permittivity of Barium Titanate Single Crystal", Czech. J. Phys., B12, 308-312 (1962).

29. A. V. Turik, "The Problem of the Surface Layer in Barium Titanate Single Crystals", Sov. Phys. Solid State 5[9] 1748-1750 (1964).

30. A. F. Devonshire, "Theory of Barium Titanate", Phil. Mag., 40[309] 1040-1063 (1949).

31. A. F. Devonshire, "Theory of Barium Titanate", Phil. Mag., 42[333] 1065-1079 (1951).

32. E. J. Huibregtse, W. H. Bessey and M. E. Dougard, "Electromechanical Behavior of Single Crystals of Barium Titanate for 25°C to

160°C", . J. Appl. Phys., 30[6] 899-905 (1959).

33. M. E. Drougard, R. Landauer and D. R. Young, "Dielectric Behavior of Barium Titanate in the Paraelectric State", Phys. Rev., 98[4] 1010-14 (1955).

34. D. Berlincourt and H. Jaffe, "Elastic and Piezoelectric Coefficients of Single-Crystal Barium Titanate", Phys. Rev.,111[1] 143-48 (1958).

35. D. A. G. Bruggeman, "Calculation of Various Physical Constants of Heterogeneous Substances:I," Ann. Phys., 24, 634-64 (1935).

36. G. Arlt and P. Sasko, "Domain Configuration and Equilibrium Domains in Barium Titanate Ceramics", J. Appl. Phys. 51[9] 4956-4960 (1980).

4. PREPARATION OF LEAD MAGNESIUM NIOBATE

4.1 General

Multilayer ceramic capacitors for electronic circuit miniaturization are attractive because of their potentially high capacitance per unit volume, together with their electrical stability, reliability, and low cost. The present material of choice for capacitors is mainly multilayer tape cast barium titanate bodies. The green sheets of modified barium titanates are cut to size, electroded, and then fired in air. The firing temperature is above 1350°C, and only expensive palladium or platinum metals can be used as internal electrodes. To reduce production

costs of terminating capacitors, new dielectric compositions with a low firing temperature ($< 1000^{\circ}C$) are being studied because at this low firing temperatures relatively cheaper Ag-Pd electrodes could be used. Complex solid solutions between ferroelectric compounds with a perovskite type structure and a general formula $Pb(B'B'')O_3$ are very attractive for this purpose. Besides a low sintering temperature, these compounds show a very high peak in the permittivity vs temperature curves [1-6].

Smolenskii, et al. [1] first reported a study on the compound $Pb(Mg^{2+}_{0.33}Nb^{5+}_{0.66})O_3$, hereafter referred to as PMN, with the perovskite crystal structure. Since then, this compound has been studied intensively by various workers. The investigations showed that the PMN system has a broad maximum of the dielectric constant just below room temperature. The magnitude of this maximum, (at 1 KHz, ~15000 for ceramic PMN and >20000 for single-crystal PMN), decreases and the temperature of this maximum increases with increasing frequency. This behavior is typical of a group of materials commonly referred to as relaxor ferroelectrics.

Recently, there has been much interest in PMN and PMN-based materials for electrostrictive applications. The electrostrictive strains generated in PMN-based ceramics are found to be an order of magnitude larger than those of TiO_2-based ceramics, due to the large dielectric constant of PMN. The induced electrostrictive strains are proportional to the square of the polarization.

The main limitation of the application of PMN in electronic devices

has been the lack of a simple, reproducible fabrication technique for pure PMN. The formation of pure perovskite PMN is difficult due to the formation of a pyrochlore type parasitic phase during fabrication. The main cause for this has been attributed to the volatilization of lead oxide during fabrication. Studies on the mechanism of formation and the ceramic processing of this system have shown that this parasite phase is very difficult to eliminate, even with an excess of PbO as regard to the stoichiometric composition [7-13].

Dielectric films produced by MOD processes are expected to have a finer grain size, more uniform surface and higher density compared to conventional tape cast films. Since the MOD films are relatively thinner it is also expected that the films produced using the MOD technique would give more capacitance per unit volume than the films produced using conventional routes.

This project involved a preliminary study of the mechanism of formation of perovskite PMN in powder and film forms using the MOD technique of fabrication. The aim was to develop procedures to obtain pyrochlore-free perovskite phase. For this purpose, phase formation as a function of precursor composition and processing conditions was studied, and an attempt was made to understand the mechanism of perovskite PMN formation. Since the elimination of pyrochlore is a crucial initial step towards the fabrication of PMN ceramics with high dielectric constant (as is evident by the difference in the ε values of single-crystal and polycrystalline ceramic PMN), attempts were made to study the crystal structure and composition of the pyrochlore phase formed during fabrication in order to gain an insight into the pyrochlore - perovskite

conversion reaction. In case of MOD films, the quality of the film being produced was also of considerable interest. The aim was to produce a film which was uniform, homogeneous and pin-hole free. For this purpose, preliminary studies were conducted on various substrates. For better quality control and consistency in the results, all the required compounds were synthesised in house.

4.2 Experimental

4.2.1 Selection of Compounds

The metallo-organic compounds selected were lead neodecanoate, magnesium neodecanoate and niobium tri-ethoxy-di-neodecanoate. The synthesis of lead neodecanoate was discussed in Section 2.2.1.3, and synthesis of the other two compounds is presented in the following sections. Individual xylene solutions of these MOD compounds were mixed in stoichiometric proportions to obtain a solution having a $Pb_3MgNb_2O_9$ composition. Xylene was chosen as the solvent because it had a low boiling point and was easily removed on heating. This 'PMN Solution' was used to study the decomposition characteristics, phase formation, and for structural studies. Some of the studies were conducted with the 'PMN Solution' having an additional amount of lead or magnesium MOD precursors to give excess PbO or MgO in the fired products.

4.2.2. Synthesis of Niobium Tri-Ethoxy-Di-Neodecanoate

Niobium tri-ethoxy-di-neodecanoate was prepared using niobium penta-ethoxide. Niobium penta-ethoxide is an extremely moisture and air

sensitive liquid, thus an inert gas atmosphere was required to transfer this substance. In a glove bag filled with nitrogen, a previously weighed 100 ml round-bottom flask with rubber septum, a bar magnet and the niobium compound in vials were placed. A vial was broken inside the glove bag and 25 grams of niobium penta-ethoxide was transferred into the flask under nitrogen. The flask was closed with the rubber stopper and weighed again to get the accurate weight of the niobium compound. The flask was then placed on a heating mantle supported over the magnetic stirrer and 84.31 ml of benzene and 30.9 ml of neodecanoic acid were added to the flask under nitrogen using a syringe. The solution was stirred and the rubber septum was quickly replaced by the condenser. The solution was heated and allowed to reflux for 4 hours. It was then filtered under a mild suction to remove suspended impurities. A pale yellow syrupy liquid of the niobium compound was obtained. The equation for the synthesis is given below.

$$Nb(OC_2H_5)_5 + 2C_9H_{19}COOH = Nb(OC_2H_5)_3(C_9H_{19}COO)_2 + 2C_2H_5OH$$
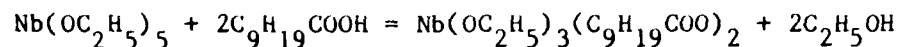
4.2.3 Synthesis of Magnesium Neodecanoate

In order to prepare a MOD precursor of magnesium, attempts were made with various inorganic compounds of magnesium such as $Mg(NO_3)_2$, $MgCO_3$, MgO etc. However, a suitable metallo-organic compound of magnesium could not be obtained. Finally, $Mg(OH)_2$ was found to give the best results as far as the clearity of the solution, and the solubility in xylene was concerned.

Fifty eight grams of $Mg(OH)_2$, 198.0 ml. of purified neodecanoic acid and about 125 ml of xylene for refluxing purpose were mixed in a round bottom flask. After connecting it to a fractional distillation assembly, the content of the flask was heated on a heating mantel. The temperature of the flask was kept constant at $95^{\circ}C$. A magnetic stirrer was used during distillation to stir the content of the flask. Water vapors and some amount of xylene were collected in a beaker as the distillation product. After about one hour, heating was stopped and the whole assembly was allowed to cool. The content of the flask was poured in a china dish, and was reheated at $135^{\circ}C$ in order to complete the reaction. The content of the china dish was dissolved in xylene and was filtered using a Buchner funnel to remove the unreacted magnesium hydroxide. A small amount of magnesium hydroxide, deposited at the bottom after 12 hours, was removed by filtering. The equation for the synthesis is given below.

$$Mg(OH)_2 + 2C_9H_{19}COOH = (C_9H_{19}COO)_2Mg + 2H_2O.$$
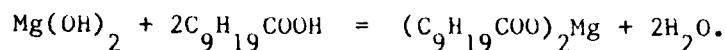
4.2.4 X-ray Diffraction Studies

Compound identification and structural studies were performed on the fired products in bulk and film forms. The x-ray diffraction technique was used to determine the phase(s) present in the fired products as a function of precursor composition and processing conditions, and if appropriate, the crystal structures of the phases formed. An automated

x-ray diffractometer was used for this purpose. The phase analysis was performed using Cu Kα radiation and 2° (2θ)/min goniometer speed.

From crystal structure analysis, the high angle reflections of the respective phases were chosen for the lattice parameter determination. The accurate peak location was determined using the program "AUTOFI" adopted for the Siemens model. This program was designed to produce an intensity profile between specified two-theta angles and then to determine the peak position for the peaks in the range. Only peaks above a user-defined background level were located to prevent random fluctuation in the background being reported as peaks. The computer program fitted the Pearson Type VII distribution, using a least-squares method to all peaks in the 2θ range. Gaussian distributions are commonly too broad near the peak and too narrow at the tails. Functions proportional to a Cauchy distribution are usually unsatisfactory in the opposite way. Pearson Type VII distributions appear to closely represent the shape of a symmetric X-ray diffraction peak [14].

The determination of lattice constants of a phase was done by using program which refines lattice constants for any symmetry by a modified least square method. With the help of this program, several types of extrapolation functions can be used either singly or in combination. In the present investigation, Nelson-Riley's extrapolation function was used. Knowing the (hkl) and determining the experimental value of 2θ and thus d, the lattice constant was calculated for each peak and plotted versus the function $1/2(\frac{\cos^2\theta}{\sin\theta} + \frac{\cos^2\theta}{\theta})$. The extrapolated value of the lattice constant corresponding to $\theta = 90^{\circ}$ gave the minimum error. A complete error treatment was made with the help of the computer.

4.2.5 Characterization of MOD Compounds

The MOD compounds of lead, magnesium and niobium were dissolved in
xylene and their decomposition behavior was studied using TGA. From the
thermograms of individual compounds, information about the final firing
temperature.   The composition of final products was determined by com-
paring the weight loss during firing with the phases identified by the
x-ray diffraction studies. The metallo-organic precursors were fired in
a platinum crucible and the fired products were analyzed for the phases
present.   The weight percent concentrations of these phases were
obtained by noting the difference in the weights of initial compounds
and that of fired products. Results from the TGA and x-ray diffraction
studies are given in Table 4.1.

4.2.6 TGA of ´PMN Solution´

The ´PMN Solution´ prepared by using MOD compounds in xylene was
studied for its decomposition behavior. The TGA was performed in the
temperature range of 27-900°C using heating rates of 1°C/min, 5°C/min
and 10°C/min. The results showed that the final decomposition tempera-
ture decreased as the heating rate decreased. The TGA results are sum-
marized in Table 4.2.

4.2.7 PMN Powder Formation

The aim of PMN firing studies in the bulk form was to develop a
procedure to obtain perovskite lead magnesium niobate with the minimum
possible pyrochlore. Three ´MOD Solutions´ were prepared, namely, a

Table 4.1   TGA and X-ray Diffraction Results of Metallo-Organic Compounds
in Xylene.

Metallo-Organic Compound	T_d^* ($^\circ$C)	Wt. % Fired Product	Fired Product
Lead Neodecanoate	415	14.2	PbO
Magnesium Neodecanoate	400	2.23	MgO
Niobium Tri-ethoxy-di-neodecanoate	400	14.0	Nb_2O_5

*: T_d: Temperature at which decomposition is complete.

Table 4.2   TGA of 'MOD Solution' of Stoichiometry PMN in Xylene.

Heating Rate	T_d^a ($^\circ$C)	Wt. % Fired Product
1°C per min.	300	15.0
5°C per min.	325	15.0
10°C per min.	375	15.0

a: T_d : Temperature at which decomposition is complete.

stoichiometric lead magnesium niobate solution in xylene (referred to as
'PMN Solution'), a 'PMN Solution' with additional 2 wt % PbO, and a 'PMN
Solution' with additional 2 wt% MgO. The 'PMN Solution' was prepared by
mixing weighed amounts of the MOD compounds of lead, magnesium and
niobium dissolved in xylene as per required for $Pb_3MgNb_2O_9$ composition.
The 'MOD Solutions' with additional 2 wt % PbO or MgO were prepared by
adding the weighed amounts of the MOD compounds of lead or magnesium, as
per the case, to the 'PMN Solution'. The fired products contained 100
parts by weight of PMN + 2 parts by weight of excess PbO or MgO if
excess were added. A small amount of the 'PMN Solution' was fired in a
platinum crucible at the firing rate of 1^oC /min to the decomposition
temperature determined by TGA, in order to determine the wt % yield of
the fired products.

The firing studies on the three above mentioned 'MOD Solutions'
were conducted by firing about 5 to 10 grams of these solutions in a
platinum crucible, using a two stage process. The initial firing at the
rate of 1^oC per minute, for firing temperatures to $^-420^o$C, was used for
all the firing schedules. This slow heating rate at the early stages of
the firing was desired because the vapor pressure of lead oxide can
cause considerable lead losses during the removal of organic compounds,
and because the final decomposition temperature to the PMN compound
decreases with decreasing heating rates. The extent of lead loss in the
form of lead oxide has a crucial effect on the formation of the
perovskite phase as opposed to the pyrochlore phases during the final
stages of firing.

The decomposition products from the initial firing were further heated from 600°C to 1100°C for times ranging from 30 min to 3 hours in order to complete the phase formation reactions. The phases in the fired samples were analyzed using x-ray diffraction with Cu Kα radiation.

4.2.8 PMN Film Processing

The second part of this project consisted of a preliminary study of the development of PMN films formed on various substrates by the decomposition of the 'MOD Solutions' prepared from metallo-organic precursors. The selection of metallo-organic decomposition technique to produce films is based on the fact that the MOD process produces a film which is denser, and more uniform in composition and microstructure. Also, the thickness of the films can be controlled easily by using this process. For the preliminary studies, the phase formation in PMN films was determined as a function of substrate materials, processing conditions and precursor compositions. The experiments that were conducted are described below.

I. In one set of experiments, xylene solutions that gave stoichiometric PMN, or PMN with excess PbO or MgO on thermal decomposition were spun on platinum foils and were fired at various temperatures. The phase formation studies were conducted using x-ray analysis, and the quality of the films were tested visually.

II. In another set of experiments, AlSiMag 838 substrates were used for film deposition. The uniformity of the films was tested by optical

microscopy and the phase formation studies were conducted using x-ray analysis.

4.2.9 Substrates

Selection of a suitable substrate was an important factor for obtaining a film with desired qualities. Several parameters were considered in the selection of a suitable substrate such as:

1) the chemistry of the substrate, because the development of film adhesion always involves some degree of chemical interaction between the film and the substrate;

2) the substrate should have a melting point well above the range of the desired working temperatures;

3) the substrate should not react with the metallo-organic compounds, producing phases that alter the properties of the film unfavorably;

4) the coefficient of thermal expansion of the substrate should be as close as possible to that of the products formed during the processing since this will affect the uniformity of the fired films;

5) the surface roughness of the substrate limits the minimum thickness of a film that can be continuous.

The preliminary studies were conducted on platinum foils (with cross-sectional area of 4 cm^2) because they eliminate the possibility of any chemical interaction with the films and thus provide good samples for structural studies. However, due to frequent shape deformation of the platinum foils during handling and also due to the high cost of the foils, the platinum foils were replaced by alumina substrates.

Alumina (96 to 99.8% Al_2O_3) is the most common material used for substrates in hybrid microelectronics because it is quite good as far as all of the general requirements are concerned. They can withstand high temperatures and are available in a number of surface roughness specifications. The AlSiMag 838 (99.5% Al_2O_3) substrates were used for the later part of this study. The surface roughness of the AlSiMag 838 substrates, measured with a profilometer, was found to be ˜0.15 μm.

4.2.10 Formation of Wet Films

The technique used for formation of wet films is an important initial stage whose selection has to be carefully considered. The thickness and the uniformity of the wet films affect all subsequent processes. The deposition of wet films on the substrate was done by spinning. This method gives a very uniform coating of a solution on a substrate. Also, layers of higher thickness can be obtained by repeated spinning operations.

The selection of proper spinning parameters, such as, the spinning speed and the spinning time, is very important. Low spinning speeds may lead to edge build up caused by the surface tension of the solution at the edge of the substrate, whereas very high speeds may cause streaking or thin coatings. Viscosity of the solution detrmines the spinning speed, and by proper selection of this parameter, coatings of various thickness can be obtained.

An LS-8000 lab spinner[*] was used during the course of this project.

---

[*] Integrated Tech. Inc.

The following procedure was used to deposit wet films. The ´MOD Solutions´ prepared for the bulk firing studies were used as the starting solutions for film deposition. The viscosities of the starting solutions were adjusted for spinning operation by removing some of the xylene by bubbling air or nitrogen through these solutions. The initial solution had the viscosity of water and after bubbling gas through it the viscosity was similar to that of a syrup. The substrate was manually centered on the chuck; the chosen spinning parameters were set; the substrate was flooded with the solution until all parts of the substrate were wet and the solution just spilled over; the substrate was rotated for the preset spinning time and speed. The selection of spinning parameters was done by trial and error for each batch of solutions. In general, the spinning speed was in the range of 1500-2000 rpm and spinning time was between 15 to 25 seconds.

4.3 Results and Discussion

4.3.1 Formation of Lead-Magnesium Niobate in Bulk Form

The results from the firing studies of the stoichiometry ´PMN Solution´ are reported in the Table 4.3. The wt % yield was obtained from the weight difference between the fired product and the starting ´Solution´. The third column in the Table 4.3 indicates the approximate percentage yield in terms of the relative contents of the perovskite phase vs. the pyrochlore phases obtained from x-ray data using the relationship given at the bottom of the Table 4.3.

The x-ray diffraction studies of the stoichiometric PMN samples

Table 4.3 Firing of Stoichiometry 'PMN Solution'.

Sample	Firing Schedule	Wt.% Yield	Vol.% PMN*
1	RT to 250°C/ 1°C/min + 250°C /2 hrs.	12.72	0
2	RT to 400°C/ 1°C/min + 400°C /2 hrs.	-	0
3	RT to 420°C/ 1°C/min	13.39	0
4	RT to 440°C/ 1°C/min	-	0
5	RT to 420°C/ 1°C/min + 500°C/2 hrs.	-	0
6	RT to 420°C/ 1°C/min + 550°C/4 hrs.	-	0
7	RT to 420°C/ 1°C/min + 640°C/2 hrs.	-	0
8	RT to 420°C/ 1°C/min + 700°C/2 hrs.	-	82
9	RT to 420°C/ 1°C/min + 800°C/2 hrs.	13.40	90
10	RT to 420°C/ 1°C/min + 875°C/2 hrs.	12.81	95
11	RT to 420°C/ 1°C/min + 900°C/3 hrs.	11.86	81
12	RT to 420°C/ 1°C/min + 1000°C/2 hrs.	11.90	69
13	RT to 420°C/ 1°C/min + 1100°C/2 hrs.	11.63	65
14	RT to 350°C/ 1°C/min + 750°C/2 hrs.	-	82

* : $Vol.\% = \left|\dfrac{Iperov.}{Iperov. + Ipyro.}\right| *100\%$

Iperov. = Peak Height of the Most Intense Perovskite Peak {hkl 110}.

Ipyro. = Peak Height of the Most Intense Pyrochlore Peak {hkl 222}.

fired in platinum crucibles were conducted using Cu Kα radiation. The phases present in various samples were identified by matching the experimental x-ray patterns with the Powder Diffraction File. The correct identification of phases in the PMN system is very difficult because: 1) the intermediate phases, termed pyrochlores, have almost identical diffraction patterns; and 2) the diffraction patterns of the starting compounds, PbO, MgO and Nb_2O_5 have sets of lines which overlap with those of the pyrochlores and perovskite, making it difficult to determine the temperatures at which the various oxides started to react or a phase change took place. A list of possible compounds present in the PMN system at various temperatures and the location of their major peaks for Cu Kα radiation is given in Table 4.4.

Other factors which further complicate the phase identification, and which are partially responsible for the conflicting results available in the published literature are:

1) the excess PbO and/or MgO added during processing might be present at high temperatures due to incomplete reactions, or simply because they were added in excess of what was actually required;

2) depending upon the processing conditions, such as, firing time and temperatures, the amount of lead loss may vary, producing different $PbO-Nb_2O_5$ based phases for different sets of experiments;

3) the excess MgO, added to reduce the pyrochlore in the final samples, might be incorporated in the various product phases and thus affect their x-ray patterns.

Table 4.4   List of the Possible Compounds Formed in the PMN System and Their Major X-ray Peak Positions.

Compound	Crystal Structure	Powder Diffraction File			
			2θ	29.95	44.4
MgO	Cubic	30-794	$d^{\circ}A$	3.05	2.05
			I	100	100
			2θ	42.95	62.35
MgO	Cubic	4-829	$d^{\circ}A$	2.106	1.489
			I	100	52
			2θ	28.65	31.85
PbO	Tetragonal	5-561	$d^{\circ}A$	3.12	2.81
			I	100	62
			2θ	29.11	30.33
PbO	Orthorhombic	5-570	$d^{\circ}A$	3.07	2.95
			I	100	31
			2θ	28.35	22.60
$(Nb_2O_5)xO$	Orthorhombic	27-1313	$d^{\circ}A$	3.15	3.93
			I	100	90
			2θ	22.50	28.40
Nb_2O_5	Monoclinic	27-1313	$d^{\circ}A$	3.95	3.14
			I	100	90
			2θ	31.15	44.60
PMN	Cubic	27-1199	$d^{\circ}A$	2.87	2.03
			I	100	41

Table 4.4 Continued.

Compound	Crystal structure	Powder Diffraction File						
			2θ	14.55	29.95	34.06	48.70	57.25
$Pb_3Nb_4O_{13}$	Cubic	25-443	$d^\circ A$	6.09	3.05	2.64	1.87	1.61
			I	<2	100	30	25	16
			hkl	111	222	400	440	533
			2θ	14.30	28.90	33.70		47.25
$Pb_3Nb_2O_8$	Tetragonal	30-712	$d^\circ A$	6.16	3.09	2.66	1.8963	1.61
			I	3	100	25	25	30
			hkl	101	202	220	224	422
			2θ	14.45	29.20	33.85	48.70	57.45
$Pb_{1.83}Nb_{1.71}Mg_{0.29}O_{6.39}$	Cubic	33-769	$d^\circ A$	6.12	3.06	2.65	1.87	1.60
			I	5	100	45	70	85
			hkl	111	222	400	440	622

The x-ray diffraction pattern of the sample 1 indicated that the decomposition of the ¨MOD Solution¨ was complete after slow 1^oC/min heating to 250^oC and holding for 2 hours, giving a mixture of the starting oxides. The broad peak observed in the 2θ range of 20-35° indicated the presence of very small particle size elemental oxides with their strongest peaks falling in this range, PbO (28.65^o for tetragonal phase and 29.11^o for the orthorhombic phase), MgO (29.95^o) and Nb_2O_5 (28.35^o for orthorhombic phase). On further heating to 400^oC and holding for 2 hours, as in the case of sample 2, the x-ray peaks for a pyrochlore phase was observed along with those for starting oxides. Samples 2 to 7, fired in the temperature range 400-640^oC indicated the pyrochlore phase along with the PbO. Other oxides, MgO and Nb_2O_5 could not be detected in the x-ray patterns, probably due to their very small particle size. The pyrochlore phase in this temperature range seems to be based on the composition $Pb_3Nb_2O_8$, although a complete matching of the patterns was not possible.

The perovskite peaks were first observed in sample 7, fired at 640°. Further increases in the firing temperature continuously increased the perovskite content with the corresponding decrease in the pyrochlores. This trend was observed in the samples 8-10 and 14, fired between the temperature range 700-875°.

The diffraction patterns of the samples 8 and 9 fired in the temperature range 700-800° indicated an extra peak at $2\theta \sim 30.5^o$. This peak disappeared as the temperature was further increased (sample 10). Except for this peak, the rest of the peaks in the x-ray patterns could be separated into two sets, the perovskite phase and the pyrochlore

phases.   Samples   11-13   fired at temperatures above 875° showed a con-
tinuous decrease in the perovskite content and a corresponding   increase
in the pyrochlores with increasing firing temperature.

The pyrochlore in the samples fired in the temperature   range   700-
1100° matches closest to a mixture of $Pb_3Nb_2O_8$ and $Pb_2Nb_2O_7$ in terms of
intensity, with the first type being the major pyrochlore phase. A   com-
plete matching of the experimental patterns with any of the listed pyro-
chlore phases was not obtained.

In summary, the x-ray diffraction and firing studies indicated that
the   perovskite   was   a major phase in the temperature range $700-1000^{\circ}C$.
The maximum in the perovskite content was   obtained   at $875^{\circ}C$, with   a
further   decrease in content as the temperature was increased due to the
lead loss at high temperatures.   It was also found that at low   tempera-
tures, pyrochlore was formed which converted into perovskite as the fir-
ing temperature was further increased.   However, the complete transition
from pyrochlore to perovskite was not observed.

The x-ray diffraction results for samples 15-18 having PMN   with   2
percent   excess   PbO   are given in Table 4.5.   Sample 15, fired at $800^{\circ}C$
for 2 hours, showed an extra peak at $^-30.5^{\circ}$, as   in   the   case   of   the
stoichiometric PMN sample fired at this temperature (sample 9). This
peak also disappeared at   higher   temperatures   (samples   16-18).   The
results   of   the experiments using ´PMN Solution with 2 wt % excess PbO´
showed that addition of extra PbO in the original solution   (to   compen-
sate for the lead loss at high temperatures) increased the amount of the
perovskite phase in the   final   product.   Pyrochlore-free   PMN   was   not

Table 4.5   Firing of 'PMN Solution with Excess 2 wt% PbO'.

Sample	Firing Schedule	Wt.% Yield	Vol.% PMN*
15	RT to 420°C/1°C/min + 800°C/2 hrs.	–	93
16	RT to 420°C/1°C/min + 875°C/2 hrs.	12.96	98
17	RT to 420°C/1°C/min + 1000°C/2 hrs.	12.34	76
18	RT to 420°C/1°C/min + 1100°C/2 hrs.	11.03	93

$$* : Vol.\% = \left| \frac{Iperov.}{Iperov. + Ipyro.} \right| *100\%$$

Iperov. = Peak Height of the Most Intense Perovskite Peak {hkl 110}.

Ipyro. = Peak Height of the Most Intense Pyrochlore Peak {hkl 222}.

obtained in any of the samples, but the sample 16 showed 98 vol % PMN.

Phase formation in the 'PMN solution with excess 2 wt % MgO' was studied as a function of firing temperatures and time. It was found that the addition of excess MgO gave significantly better results in terms of pyrochlore to perovskite conversion in the temperature range of 425-1000°C, as shown in Table 4.6. The perovskite peaks were first observed at temperatures as low as 420°C (sample 19). It was also observed that the reaction product of the 'PMN Solution with 2 wt.% excess MgO' fired to 420°C at the rate of 1°C per min. followed by additional heating of 2 hours at 875°C (sample 21) did not indicate the presence of any pyrochlore phase in the x-ray diffraction pattern.

The perovskite PMN obtained from the PMN solution with excess of two percent MgO was used for determination of lattice constant. The lattice constant of this phase was found to be a = 0.4038 nm.

4.3.2 PMN Films

The x-ray diffraction results for films fired on platinum substrates are given in Table 4.7. The results of preliminary studies for deposition of PMN on platinum foils indicated that the removal of organic substances from the wet films was complete by 300°C producing an amorphous film, as was shown by the powder diffraction pattern of sample 24. A broad peak was observed at 2θ ~30° indicating the presence of lead, magnesium and niobium oxides in very fine particle size. On increasing the firing temperature to 520°C, as in the case of sample 25, the formation of the pyrochlore could be observed in the x-ray diffrac-

Table 4.6 Firing of 'PMN Solution with Excess 2 wt% MgO'.

| Sample	Firing Schedule	Vol. % PMN[*]	Figure No.[**]
19	RT to 420°C/ 1°C/ min + 420°C/2 hrs.	18	4.19
20	RT to 420°C/ 1°C/ min + 800°C/2 hrs.	97	4.20
21	RT to 420°C/ 1°C/ min + 875°C/2 hrs.	100	4.21
22	RT to 420°C/ 1°C/ min + 1000°C/2 hrs.	69	4.22
23	RT to 420°C/ 1°C/ min + 1100°C/2 hrs.	65	4.23

$$* : Vol.\% = \left| \frac{Iperov.}{Iperov. + Ipyro.} \right| * 100\%$$

Iperov. = Peak Height of the Most Intense Perovskite Peak {hkl 110}.

Ipyro. = Peak Height of the Most Intense Pyrochlore Peak {hkl 222}.

** : XRD Patterns are in Appendix D.

Table 4.7 Firing of Stoichiometry Film of PMN on Platinum Substrates.

Sample	Firing Schedule	Vol.% PMN*
24	RT to 300°C/ 1°C per min.	0
25	RT to 520°C/ 1°C per min.	0
26	RT to 620°C/ 1°C per min.	~0
27	RT to 800°C/ 1°C per min.	
	+ 800°C/ 2 hr	94

* : $Vol.\% = \left| \dfrac{Iperov.}{Iperov. + Ipyro.} \right| *100\%$

Iperov. = Peak Height of the Most Intense Perovskite Peak {hkl 110}.

Ipyro. = Peak Height of the Most Intense Pyrochlore Peak {hkl 222}.
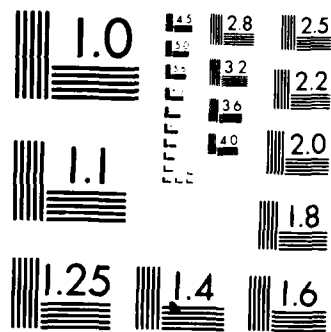
MICROCOPY RESOLUTION TEST CHART

NATIONAL BUREAU OF STANDARDS 1963 A

tion pattern. The x-ray pattern for pyrochlore in this case was found to be similar to that for powder samples. The perovskite peaks were first observed in the sample 26, fired to 620°C at the rate of 1°C per min. On further increasing the firing temperature, the pyrochlore content of the sample decreased with a corresponding increase in the perovskite, as shown for sample 27.

In summary, the best result was obtained with the film fired, first, continuously up to 800°C and then, for 1 hour at 800°C. However, the complete elimination of pyrochlore was not observed for any of the firing schedules. It was also noted that the films fired up to temperatures higher than 800°C (e.g. 875°C) showed relatively lesser amounts of perovskite than those fired up to 800°C. Also, as the firing time was increased (e. g. at 875°C), the amount of perovskite further decreased indicating that at higher temperatures the excessive lead loss took place.

4.4 Summary

1. The MOD precursors of lead, magnesium and niobium were prepared and characterized by thermogravimetric analysis. The lead neodecanoate, magnesium neodecanoate and niobium tri-ethoxy-dineodecanoate were found to have almost the same temperature ranges of decomposition and peak decomposition temperatures of 415°C, 400°C and 400°C respectively. This is advantageous since the decomposition products of the three compounds would form simultaneously giving a uniform final fired product.

2. For the purpose of firing and x-ray diffraction studies, three 'MOD Solutions' in xylene having stoichiometric PMN, PMN with 2 wt % excess PbO, and PMN with 2 wt % excess MgO compositions were prepared by mixing the MOD precursors of the lead, magnesium and niobium in the required proportions. The TGA of the 'MOD Solution' having stoichiometric PMN composition indicated that the decomposition temperature of this solution was 375°C, which is lower than those for the elemental MOD precursors used for preparing this solution.

3. The firing studies of the 'MOD Solutions' indicated that the optimum firing schedule, to obtain perovskite as the major phase and to have low lead losses in the form of lead oxide evaporation, was an initial firing to 420°C at the rate of 1°C followed by a further heating in the temperature range 700-1000°C for some constant interval of time ranging from 30 min. to 3 hours.

4. The firing studies of the stoichiometric 'PMN Solution' in bulk as well as film forms indicated that pyrochlore was the first product as the solid state reaction between the decomposed oxides of the lead, manesium and niobium took place. The pyrochlore phases formed in the powder samples and in the films had similar difraction patterns.

5. As the firing temperature of the 'PMN Solution' was increased, the low temerature pyrochlore phases converted into the perovskite lead magnesium niobate phase. This trend was continuous to approximately 800-875°C for the bulk and film samples. Beyond this tem-

perature range, the pyrochlore content of the samples increased due to the excessive lead loss.

6. Both the films and the powder samples of the stoichiometric ´PMN Solution´ did not produce a pyrochlore-free perovskite phase irrespective of the firing time and temperatures. The maximum PMN was 95 vol. % in the bulk and 94 vol. % in the films.

7. The addition of 2 wt % excess PbO increased the perovskite content in the samples with the maximum at 875°C of 98%. However, the pyrochlore phases could not be eliminated completely.

8. In case of ´PMN solution with excess 2 wt % MgO´, it was found that the addition of excess MgO gave significantly better results in terms of pyrochlore to perovskite conversion in the temperature range of $425-1000^{\circ}$C. The perovskite peaks were first observed at temperature as low as 420°C. The X-ray diffraction pattern of the reaction product of ´PMN Solution with 2 wt.% excess MgO´ fired from RT to 420°C at the rate of 1°C per min followed by an additional heating of 2 hours at 875°C did not indicate the presence of any pyrochlore phase. Traces of uncombined MgO were observed in the powder diffraction pattern of this sample, indicating that even less than 2 % excess MgO could be sufficient to eliminate most of the pyrochlore phases.

4.5. References

1. G.A. Smolenskii and A. I. Agranovskaya, "Dielectric Polarization

and Losses of Some Complex Compounds", Sov. Phys. Tech. Phys., 3, 1380, 1958.

2. G.A. Smolenskii et al., "On the Mechanism of Polarization in Solid Solutions of PNN-PMN.", Soviet Phys.-Solid State, 1, 147, 1959.

3. G.A. Smolenskii and A. I. Agranovskaya, Sov. Phys., Solid State, 1, 1429, 1960.

4. V.A. Bokov and I.E. Mylnikova, "Electrical and Optical Properties of Single Crystals of Ferroelectrics with a Diffused Phase Transition", Soviet Physics- Solid State, 3(3), 613, 1961.

5. G.A. Smolenskii, A. I. Agranovskaya, S. N. Popov and V. A. Isupov, Sov. Phys., Tech. Phys., 3, 1981, 1958.

6. F. S. Galasso, "Structure, properties and preparation of perovskite-like compounds", Pergamon Press Ltd., Oxford, 1969.

7. M. Inada, Japanese National Technical Report, 23(1), 95, 1977.

8. C.G.F. Stenger and A.J. Burggraaf, "Order and Disorder Reactions in the Ferroelectric Perovskites $Pb(Sc-Nb)O_3$ and $Pb(Sc-Ta)O_3$", Phys. Stat. Sol.(a), 61, 275, 1980.

9. S. L. Swartz and T.R. Shrout, "Fabrication of Perovskite PMN", Mat. Res. Bull., 17, 1245, 1982.

10. M. Lejeune and J.P. Boilot, "Formation Mechanism and Ceramic Process of the Ferroelectric Perovskites:PMN and PFN", Ceramics International, 8(3), 99, 1982.

11. M. Lejeune and J. P. Boilot, "Optimization of Dielectric Properties of Lead-Magnesium Niobate Ceramics", Am. Ceram. Soc. Bull., 65(4), 679, 1986.

12. S.L. Swartz et al., "Dielectric Properties of Lead-Magnesium Niobate Ceramics", J. Am. Ceram. Soc., 67(5), 311, 1984.

13. J.P. Guha, "Comment on `Dielectric Properties of Lead-Magnesium Niobate Ceramics'", J. Am. Ceram. Soc., 68(3), C-86, 1985.

14. P. G. Winchell, et al., "The Approximation of Symmetric X-ray Peaks by Pearson Type VII Distributions", J. Appl. Cryst., 10, 66-68, 1977.

END

DTIC

9 — 86